1 Wavelet and frame transforms originated from continuous and discrete splines

Amir Z. Averbuch and Valery A. Zheludev

New classes of diadic and triadic biorthogonal wavelets and wavelet-type frames in signal space are presented. The construction employs interpolatory filters with rational transfer functions that originate from continuous and discrete splines. These filters have linear phase. They are amenable either to fast cascading or parallel recursive implementation. The wavelets are applied to compression of still images, where they demonstrate a superb efficiency. Robust error recovery algorithms presented utilize the redundancy inherent in frame expansions. Experimental results recover images when (as much as) 60% of the expansion coefficients are either lost or corrupted. The proposed approach inflates the size of the image through framelet expansion and multilevel decomposition, thus providing redundant representation of the image.

1.1. Introduction

We present in this paper a few dyadic and triadic wavelet transforms and a family of wavelet frame transforms, which are generated by critically sampled (wavelets) or oversampled (frames) perfect reconstruction filter banks. The design of these generating filter banks is based on the following simple insertion rule: we construct a spline that interpolates a signal on a sparse grid and predict (approximate) missing samples by the values of the spline at corresponding points.

The goal of this paper is to demonstrate that this obvious idea has a diversity of implications and produces a set of tools that perfectly matches the needs of signal processing.

Most (but not all) of the results in the paper were presented in more details in our recent publications [1–10]. The outline of the results on triadic wavelet transforms is presented here for the first time. A detailed presentation is on the way.

Currently, there is no need to describe the importance of the wavelet transforms for signal processing. A wide variety of orthogonal and biorthogonal wavelets was designed since the famous Daubechies construction was presented in [18]. However, only few of them possess a combination of properties that are valuable

for signal and image processing: symmetry, interpolation, fair time-domain localization and smoothness of the synthesis waveforms, flat spectra, and any number of vanishing moments. The biorthogonal wavelets that we describe in the paper meet these requirements. Dyadic wavelets based on the discrete splines are closely related to the popular Butterworth filters. Dyadic synthesis wavelets based on the continuous splines of even order are the splines themselves. However, synthesis wavelets based on the splines of odd order form a new class of functions that are smoother than the generating splines.

These biorthogonal wavelets were tested for compression of still images. After the multiscale transform, the coefficients are coded using the SPIHT algorithm by Said and Pearlman [41] followed by arithmetic coding. The results on benchmark images demonstrated that the designed wavelet transforms are competitive with the popular B9/7 biorthogonal transform [15, 31], which is the core of the JPEG 2000 image compression standard. Note that the compression results in the paper differ from the compression results reported in our previous paper [7], where arithmetic coding was not used.

The theory of wavelet frames or framelets is an extension of wavelet analysis. Currently, it is a subject of extensive investigation by researchers working in signal processing and applied mathematics. A wavelet frame is generated by several mother wavelets and provides a redundant expansion of a function or a signal. Due to this redundancy, there is more freedom in the design and implementation of the frame transforms. The frame expansions of signals demonstrate resilience to quantization noise and to coefficients losses [23, 24, 29]. Thus, frames may serve as a tool for error correction in signals transmitted through lossy channels. Actually, the frame transforms of multimedia signals can be interpreted as joint source-channel encoding for lossy channels, which are resilient to quantization noise and erasures. This approach was developed in [21, 25, 32, 33]. Due to additional adaptation capabilities, the overcomplete representation of signals has a potential to succeed in feature extraction and identification of signals. Promising results on image reconstruction are recently reported in [1, 12, 13].

A common approach to construction of a framelet system in the function space L^2 starts from the introduction of a pair of refinable functions (or one function), which generate(s) multiresolution analysis in L^2. Then, the wavelets are derived by one or another method as linear combinations of refinable functions. Many construction schemes are based on unitary extension principle [40] for tight frames and mixed extension principle [39] for biframes. These principles reduce the construction of a framelet system to the design of a perfect reconstruction filter bank. The masks of the given refinable functions serve as lowpass filters in the filter bank.

On the other hand, the oversampled perfect reconstruction filter banks by themselves generate wavelet-type frames in signal space [16, 26]. We use filter banks as an engine to construct a new family of frames in the signal space. Under some relaxed conditions, infinite iterations of the frame filter banks result in limit functions, the so-called framelets, which generate the wavelet frames in L^2. The framelets are symmetric, interpolatory, and have flat spectra combined with

fine time-domain localization and efficient implementation of the transforms. The framelets are smooth and may have any number of vanishing moments. The redundancy rate is two.

Recently, a new oblique extension principle (OEP) was proposed [20], which essentially extends the tools for design of wavelet frames in L^2. New wavelet frames with advanced properties were constructed using OEP. However, the OEP scheme operates with filter banks that lack perfect reconstruction property. Therefore, these filter banks do not generate frames in signal space that is our prime goal.

We propose to use the wavelet frames (framelets) presented in this paper as a tool for error correction for signals transmitted through lossy channels. These frames provide minimal redundancy. The simplicity and low complexity involved in the decomposition and reconstruction of the designed frame transforms give rise to efficient joint source-channel coding and decoding. Their properties promise good error recovery capabilities. Results of our experiments with erasure recovery for multimedia images confirm this claim. It is shown by means of simulations that these framelets can effectively recover from random losses that are close to the theoretical limit.

We present also a new family of the so-called triadic biorthogonal wavelets, which, unlike the commonly used diadic wavelets, have dilation factor of 3. They originate from the insertion rule, where two missed samples are predicted by interpolatory spline. Unlike dyadic wavelet transforms, one step of the triadic transform splits the frequency domain into three subbands. Three waveforms participate in the expansion of a signal. This promises better adaptivity of the expansion to the properties of the signal. A useful property of the transforms derived from the continuous splines is that the corresponding waveforms are splines.

A similar approach can be applied to the construction of multiwavelets and multiwavelet frames, where Hermite interpolatory splines are used as a source for the design of filters. The results are presented in [6, 8].

Unlike most schemes for the construction of wavelets and wavelet frames, we use infinite impulse response (IIR) filters with rational transfer functions. Consequently, the corresponding waveforms do not have compact support. But this fact should hardly be counted as a drawback because of the exponential decay of the waveforms as the argument grows. As for the implementation, it can be carried out in a fast recursive mode. On the other hand, usage of IIR filters enables to achieve a combination of properties, which are impossible to get with finite impulse response (FIR) filters. For example, currently, only (anti)symmetric framelets with 3 vanishing moments are designed [28, 42]. But, using IIR filters, we succeeded in design of symmetric framelets with any number of vanishing moments.

Note that wavelet constructions that are based on filter banks with rational transfer functions were originally introduced in [27]. In particular, nonsymmetric wavelets, which are based on causal Butterworth filters, were presented in [27]. Petukhov [36] designed a family of symmetric wavelets with rational symbols and applied them to video compression [17].

The paper is organized as follows. In Section 1.2, we describe some known facts about filter banks and splines. In Section 1.3, we present prediction filters

that originate from continuous and discrete splines. Section 1.4 describes the lifting scheme for the design and implementation of diadic wavelet transforms and presents the corresponding filter banks. In Section 1.5, we present results of the experiments in image compression using the designed diadic wavelets. In Section 1.6, we explain the construction of interpolatory wavelet frames using spline-based filter banks, whereas in Section 1.7 these frames are applied to the erasure correction in transmitted signals. Section 1.8 is devoted to the design of triadic biorthogonal wavelet transforms. In the appendix, we outline the recursive implementation of IIR filters.

1.2. Preliminaries

In this section we describe some known facts about filter banks and splines that are used in the sequel.

1.2.1. Filter banks

We call the sequences $\mathbf{x} \triangleq \{x(n)\}$, $n \in \mathbb{Z}$, which belong to the space l_1, (and, consequently, to l_2) discrete-time signals. The z-transform of a signal $\mathbf{x}$ is defined as $X(z) \triangleq \sum_{n\in\mathbb{Z}} z^{-n}x(n)$. Throughout the paper, we assume that $z = e^{j\omega}$.

The input $x(n)$ and the output $y(n)$ of a linear discrete time shift-invariant system are linked by the discrete convolution $y(n) = \sum_{l\in\mathbb{Z}} h(n-l)x(l)$. This processing of the signal $\mathbf{x}$ is called digital filtering and the sequence $\{h(n)\}$ is called the impulse response of the filter $\mathbf{h}$. Its z-transform $H(z) \triangleq \sum_{n\in\mathbb{Z}} z^{-n}h(n)$ is called the transfer function of the filter. Usually, a filter is designated by its transfer function $H(z)$. The function $\widehat{H}(\omega) = H(e^{j\omega n})$ is called the frequency response of the digital filter.

If filtering a signal is accompanied by downsampling of upsampling, then it is called multirate filtering. For example, application to the signal $\mathbf{x}$ of the time-reversed filter $\widetilde{\mathbf{h}}$ followed by downsampling of factor N is $\widetilde{y}(l) = \sum_{n\in\mathbb{Z}} \widetilde{h}(n - Nl)x(n)$. Application to the signal $\mathbf{y}$ that is upsampled by factor N of the filter $\mathbf{h}$ is

$$\widehat{x} = \sum_{n\in\mathbb{Z}} h^k(l - Nn)y(n) \Longleftrightarrow X(z) = H(z)Y\left(z^N\right). \tag{1.1}$$

The set of filters $\{\widetilde{H}^k(z) = \sum_{n\in\mathbb{Z}} z^{-n}\widetilde{h}^k(n)\}_{k=0}^{K-1}$, which, being time-reversed and applied to the input signal $\mathbf{x}$, produces the set of decimated output signals $\{\widetilde{\mathbf{y}}^k\}_{k=0}^{K-1}$,

$$\widetilde{y}^k(l) = \sum_{n\in\mathbb{Z}} \widetilde{h}^k(n - Nl)x(n), \quad k = 0,\ldots,K-1, \tag{1.2}$$

is called the K-channel analysis filter bank. Here $N \in \mathbb{N}$ is the downsampling factor. The set of filters $\{H^k(z) = \sum_{n\in\mathbb{Z}} z^{-n}h^k(n)\}_{k=0}^{K-1}$, which, being applied to the

set of input signals $\{\mathbf{y^k}\}_{\mathbf{k=0}}^{\mathbf{K-1}}$ that are upsampled by factor N, produces the output signal $\hat{\mathbf{x}}$,

$$\hat{x}(l) = \sum_{k=0}^{K-1} \sum_{n\in\mathbb{Z}} h^k(l - Nn) y^k(n), \quad l \in \mathbb{Z}, \tag{1.3}$$

is called the K-channel synthesis filter bank. If the upsampled signals $\tilde{\mathbf{y}}^{\mathbf{k}}$, $k = 0, \ldots, K-1$, are used as an input to the synthesis filter bank and the output signal $\hat{\mathbf{x}} = \mathbf{x}$, then the pair of analysis-synthesis filter banks forms a perfect reconstruction (PR) filter bank. If the number of channels K equals the downsampling factor N, then the filter bank is said to be critically sampled. If $K > N$, then the filter bank is oversampled. Note that critically sampled PR filter banks are used in wavelet analysis, while oversampled PR filter banks serve as a source for the design of frames.

Polyphase representation provides tools to handle multirate filtering. Let $\mathbf{x} = \{x(k)\}_{k\in\mathbb{Z}}$ be a signal. The sequences $\mathbf{x}(n)^N \triangleq \{x_{kN+n}\}_{k\in\mathbb{Z}}$, $n = 0, \ldots, N-1$, are called the polyphase components of the signal $\mathbf{x}$. Their z-transforms are denoted either by $X_{n,N}(z)$ or, when it does not lead to confusion, simply by $X(n)(z)$. Similarly, we denote the polyphase components of a filter $H(z)$ either by $H_{n,N}(z)$ or by $H(n)(z)$. The z-transforms are represented through the polyphase components:

$$X(z) = \sum_{n=0}^{N-1} z^{-n} X_{n,N}(z^N). \tag{1.4}$$

Then, the filtering can be expressed in polyphase form. We apply the time-reversed filter $\tilde{\mathbf{h}}$ to the signal $\mathbf{x}$. In the z-domain, we have

$$\begin{aligned} \tilde{Y}(z) &= \sum_{m,n=0}^{N-1} z^{m-n} H_{m,N}(z^{-N}) X_{n,N}(z^N) \\ &= \sum_{r=0}^{N-1} z^{-r} \sum_{m=0}^{N-1} H_{m,N}(z^{-N}) X_{m+r,N}(z^N) \\ &= \sum_{r=0}^{N-1} z^{-r} \tilde{Y}_{r,N}(z^N). \end{aligned} \tag{1.5}$$

Thus, the polyphase components of the output are

$$\tilde{Y}_{r,N}(z) = \sum_{m=0}^{N-1} H_m\left(\frac{1}{z}\right) X_{m+r,N}(z), \quad r = 0, \ldots, N-1. \tag{1.6}$$

If filtering is followed by downsampling, then we retain only zero-polyphase component:

$$\widetilde{y}(l) = \sum_{n\in\mathbb{Z}} \widetilde{h}(n-Nl)x(n) \Longleftrightarrow \widetilde{Y}(z) = \sum_{m=0}^{N-1} H_m\left(\frac{1}{z}\right)X_m(z). \tag{1.7}$$

If filtering is applied to the upsampled signal $\mathbf{y}$ as in (1.1), then the polyphase components of the output are

$$\widehat{X}_{n,N}(z) = H_{n,N}(z)Y(z^N). \tag{1.8}$$

Equations (1.2)–(1.8) imply the following representation for the application of the analysis and synthesis filter banks:

$$\begin{pmatrix} \widetilde{Y}^0(z) \\ \widetilde{Y}^1(z) \\ \vdots \\ \widetilde{Y}^{K-1}(z) \end{pmatrix} = \widetilde{\mathbf{P}}\left(\frac{1}{z}\right)\cdot \begin{pmatrix} X_0(z) \\ X_1(z) \\ \vdots \\ X_{N-1}(z) \end{pmatrix}, \qquad \begin{pmatrix} \widehat{X}_0(z) \\ \widehat{X}_1(z) \\ \vdots \\ \widehat{X}_{N-1}(z) \end{pmatrix} = \mathbf{P}(z)\cdot \begin{pmatrix} Y^0(z) \\ Y^1(z) \\ \vdots \\ Y^{K-1}(z) \end{pmatrix}, \tag{1.9}$$

where the $K \times N$ analysis polyphase matrix is

$$\widetilde{\mathbf{P}}(z) \triangleq \begin{pmatrix} \widetilde{H}_0^0(z) & \widetilde{H}_1^0(z) & \cdots & \widetilde{H}_{N-1}^0(z) \\ \widetilde{H}_0^1(z) & \widetilde{H}_1^1(z) & \cdots & \widetilde{H}_{N-1}^1(z) \\ \vdots & \vdots & \vdots & \vdots \\ \widetilde{H}_0^{K-1}(z) & \widetilde{H}_1^{K-1}(z) & \cdots & \widetilde{H}_{N-1}^{K-1}(z) \end{pmatrix} \tag{1.10}$$

and the $N \times K$ synthesis polyphase matrix is

$$\mathbf{P}(z) \triangleq \begin{pmatrix} H_0^0(z) & H_0^1(z) & \cdots & H_0^{K-1}(z) \\ H_1^0(z) & H_1^1(z) & \cdots & H_1^{K-1}(z) \\ \vdots & \vdots & \vdots & \vdots \\ H_{N-1}^0(z) & H_{N-1}^1(z) & \cdots & H_{N-1}^{K-1}(z) \end{pmatrix}. \tag{1.11}$$

The condition for the analysis-synthesis pair of filter banks to form a PR filter bank is

$$\mathbf{P}(z)\cdot\widetilde{\mathbf{P}}(z) = \mathbf{I}_N, \tag{1.12}$$

where $\mathbf{I}_N$ is the $N \times N$ identity matrix.

1.2.2. Bases and frames generated by filter banks

Oversampled PR filter banks form frames in the signal space, whereas critically sampled PR filter banks form biorthogonal bases.

Definition 1.1. A system $\widetilde{\Phi} \triangleq \{\widetilde{\phi}_j\}_{j\in\mathbb{Z}}$ of signals forms a frame of the signal space if there exist positive constants A and B such that for any signal $\mathbf{x} = \{x(l)\}_{l\in\mathbb{Z}}$,

$$A\|\mathbf{x}\|^2 \le \sum_{j\in\mathbb{Z}} \left|\langle \mathbf{x}, \widetilde{\phi}_j\rangle\right|^2 \le B\|\mathbf{x}\|^2. \tag{1.13}$$

If the frame bounds A and B are equal to each other, then the frame is said to be tight.

If the system $\widetilde{\Phi}$ is a frame, then there exists another frame $\Phi \triangleq \{\phi_i\}_{i\in\mathbb{Z}}$ of the signals space such that any signal $\mathbf{x}$ can be expanded into the sum $\mathbf{x} = \sum_{i\in\mathbb{Z}}\langle \mathbf{x}, \widetilde{\phi}_i\rangle\phi_i$. The analysis $\widetilde{\Phi}$ and synthesis Φ frames can be interchanged. Together they form the so-called biframe. If the frame is tight, then Φ can be chosen as $\Phi = c\widetilde{\Phi}$.

If the elements $\{\widetilde{\phi}_j\}$ of the analysis frame $\widetilde{\Phi}$ are linearly independent, then the synthesis frame Φ is unique, its elements $\{\phi_j\}$ are linearly independent, and the frames $\widetilde{\Phi}$ and Φ form a biorthogonal basis of the signal space.

Let the analysis $\{\widetilde{H}^k(z)\}_{k=0}^{K-1}$ and the synthesis $\{H^k(z)\}_{k=0}^{K-1}$ filter banks form a PR filter bank. Then,

$$\begin{aligned} x(l) &= \sum_{k=0}^{K-1}\sum_{n\in\mathbb{Z}} h^k(l-Nn)\widetilde{y}^{k,1}(n), \quad l\in\mathbb{Z}, \\ \widetilde{y}^{k,1}(l) &= \sum_{n\in\mathbb{Z}} \widetilde{h}^k(n-Nl)x(n), \quad k = 0,\dots,K-1. \end{aligned} \tag{1.14}$$

We denote for $k = 0,\dots,K-1$ that $\widetilde{\varphi}^{k,1} \triangleq \{\widetilde{\varphi}^{k,1}(l) = \widetilde{h}^k(l)\}_{l\in\mathbb{Z}}$ and $\varphi^{k,1} \triangleq \{\varphi^{k,1}(l) = h^k(l)\}_{l\in\mathbb{Z}}$, where $\{\widetilde{h}^k(l)\}$ and $\{h^k(l)\}$ are the impulse responses of the filters $\widetilde{H}^k(z)$ and $H^k(z)$, respectively. Then, (1.14) can be rewritten as

$$\begin{aligned} \mathbf{x} &= \sum_{k=0}^{K-1} \mathbf{x}^{k,1}, \quad \mathbf{x}^{k,1} \triangleq \sum_{n\in\mathbb{Z}} \widetilde{y}^{k,1}(n)\varphi^{k,1}(\cdot - Nn), \\ \widetilde{y}^{k,1}(n) &= \langle \mathbf{x}, \widetilde{\varphi}^{k,1}(\cdot - Nn)\rangle, \quad k = 0,\dots,K-1. \end{aligned} \tag{1.15}$$

Thus, the system $\widetilde{\Phi} \triangleq \{\widetilde{\varphi}^{k,1}(\cdot - Nn)\}_{n\in\mathbb{Z}}, k = 0,\dots,K-1$, of N-sample translations of the signals $\widetilde{\varphi}^{k,1}$ forms an analysis frame of the signal space. The system $\Phi \triangleq \{\varphi^{k,1}(\cdot - Nn)\}_{n\in\mathbb{Z}}$, $k = 0,\dots,K-1$, of N-sample translations of the signals $\varphi^{k,1}$ forms a synthesis frame of the signal space. Together $\widetilde{\Phi}$ and Φ form a biframe. In a special case when the filter banks are critically sampled, that is $K = N$, the pair $\widetilde{\Phi}$ and Φ forms a biorthogonal basis.

1.2.3. Multiscale transforms and discrete-time wavelets

As it is common in wavelet and framelet transforms, one of the filters in each filter bank is lowpass. We denote these filters by $\widetilde{H}^0(z)$ and $H^0(z)$. To expand the transform to a coarse scale, the analysis filter bank is applied to the output $\widetilde{y}^{0,1}(l) = \sum_{n\in\mathbb{Z}} \widetilde{\varphi}^0(n - Nl)x(n)$ from the lowpass filter $\widetilde{H}^0(z)$. Then, we have

$$\begin{aligned}
\widetilde{y}^{k,2}(l) &= \sum_{n\in\mathbb{Z}} \widetilde{h}^k(n - Nl)\widetilde{y}^{0,1}(n) = \sum_{n\in\mathbb{Z}} \widetilde{h}^k(n - Nl) \sum_{m\in\mathbb{Z}} \widetilde{\varphi}^{0,1}(m - Nn)x(m) \\
&= \sum_{m\in\mathbb{Z}} x(m) \sum_{n\in\mathbb{Z}} \widetilde{h}^k(n - Nl)\widetilde{\varphi}^{0,1}(m - Nn) = \sum_{m\in\mathbb{Z}} x(m)\widetilde{\varphi}^{k,2}(m - N^2 l) \\
&= \langle \mathbf{x}, \widetilde{\varphi}^{k,2}(\,\cdot\, - N^2 l)\rangle, \quad k = 0,\dots,K-1, \\
\widetilde{\varphi}^{k,2}(m) &\triangleq \sum_{n\in\mathbb{Z}} \widetilde{h}^k(n)\widetilde{\varphi}^{0,1}(n - Nm).
\end{aligned} \tag{1.16}$$

On the other hand, the array $\{\widetilde{y}^{0,1}(l)\}$ is restored as follows:

$$\widetilde{y}^{0,1}(l) = \sum_{k=0}^{K-1} \sum_{n\in\mathbb{Z}} h^k(l - Nn)\widetilde{y}^{k,2}(n), \quad l \in \mathbb{Z}, \tag{1.17}$$

and subsequently, the low-frequency component of the signal $\mathbf{x}$ is

$$\begin{aligned}
x^{0,1}(m) &= \sum_{l\in\mathbb{Z}} \widetilde{y}^{0,1}(l)\varphi^{0,1}(m - Nl) = \sum_{l\in\mathbb{Z}} \sum_{k=0}^{K-1} \sum_{n\in\mathbb{Z}} h^k(l - Nn)\widetilde{y}^{k,2}(n)\varphi^{0,1}(m - Nl) \\
&= \sum_{k=0}^{K-1} \sum_{n\in\mathbb{Z}} \widetilde{y}^{k,2}(n)\varphi^{k,2}(m - N^2 n), \\
\varphi^{k,2}(l) &\triangleq \sum_{n\in\mathbb{Z}} h^k(n)\varphi^{0,1}(n - Nl).
\end{aligned} \tag{1.18}$$

As a result, we have the following expansion of the signal $\mathbf{x}$:

$$\mathbf{x} = \sum_{k=0}^{K-1} \sum_{n\in\mathbb{Z}} \widetilde{y}^{k,2}(n)\varphi^{k,2}(\,\cdot\, - N^2 n) + \sum_{k=1}^{K-1} \sum_{n\in\mathbb{Z}} \widetilde{y}^{k,1}(n)\varphi^{k,1}(\cdot - Nn). \tag{1.19}$$

Next step consists of the application of the filter bank to the array $\{\widetilde{y}^{0,2}(l)\}$ and so on. After J iterations, the signal $\mathbf{x}$ appears expanded as follows:

$$\begin{aligned}\mathbf{x} = &\sum_{n\in\mathbb{Z}} \langle \mathbf{x}, \widetilde{\varphi}^{0,J}(\,\cdot\, - N^J n)\rangle \varphi^{0,J}(\,\cdot\, - N^J n) \\ &+ \sum_{j=1}^{J}\sum_{k=1}^{K-1}\sum_{n\in\mathbb{Z}} \langle \mathbf{x}, \widetilde{\varphi}^{k,j}(\,\cdot\, - N^j n)\rangle \varphi^{k,j}(\,\cdot\, - N^j n),\end{aligned} \tag{1.20}$$

where

$$\widetilde{\varphi}^{k,j}(m) \triangleq \sum_{n\in\mathbb{Z}} \widetilde{h}^k(n)\widetilde{\varphi}^{0,j-1}(n - Nm), \qquad \varphi^{k,j}(m) \triangleq \sum_{n\in\mathbb{Z}} h^k(n)\varphi^{0,j-1}(n - Nm). \tag{1.21}$$

We call the signals $\widetilde{\varphi}^{k,j}$ and $\varphi^{k,j}$ the analysis and synthesis discrete-time wavelets of jth scale, respectively. Equation (1.20) implies that shifts of the discrete-time wavelets form a biframe (biorthogonal basis) of the space of signals.

Scaling functions and continuous wavelets. It is well known (see [19]) that under certain conditions, the lowpass filter $H(z)$, such that $H(1) = 1$, generates a continuous scaling function $\varphi(t)$. To be specific, if the infinite product $\lim_{S\to\infty}\prod_{\nu=1}^{S} H(e^{\omega 2^{-\nu}\omega})$ converges to a function $\Phi(\omega) \in L^2(\mathbb{R})$, then the inverse Fourier transform of $\Phi(\omega)$ is the scaling function $\varphi(t) \in L^2(\mathbb{R})$, which is the solution to the refinement equation $\varphi(t) = 2\sum_{n\in\mathbb{Z}} h(n)\varphi(2t - n)$. Similarly, if the infinite product $\lim_{S\to\infty}\prod_{\nu=1}^{N} H(e^{\omega N^{-\nu}\omega})$ converges to a function $\Phi(\omega) \in L^2(\mathbb{R})$, then the inverse Fourier transform of $\Phi(\omega)$ is the scaling function $\varphi(t) \in L^2(\mathbb{R})$, which is a solution to the refinement equation $\varphi(t) = 2\sum_{k\in\mathbb{Z}} h_k\varphi(Nt - k)$. Thus, the refinement equation results in dilation with factor N for the scaling function $\varphi(t)$.

Assume that the lowpass analysis filter $\widetilde{H}^0(z)$ generates the analysis scaling function $\widetilde{\varphi}(t)$. If the impulse responses of the filters $\widetilde{H}^k(z)$, $k = 1,\ldots,K-1$, are finite or decay exponentially, then the continuous functions $\widetilde{\psi}^k(t) \triangleq \sum_{n\in\mathbb{Z}} \widetilde{h}^k(n)\widetilde{\varphi}(Nt - n)$ are called the continuous analysis wavelets with dilation factor N.

A wavelet $\widetilde{\psi}^k(t)$ has p vanishing moments if $\int_{-\infty}^{\infty} t^s\widetilde{\psi}^k(t)dt = 0, s = 0,\ldots,p-1$. The number of vanishing moments of the wavelet $\widetilde{\psi}^k(t)$ is equal to the multiplicity of zero of the filter $\widetilde{H}^k(z)$ at $z = 1$ (see [43]). The same facts hold for the synthesis filter bank $H^k(z)$, $k = 0,\ldots,K-1$.

We consider in this paper the cases $N = 2$ (diadic wavelets) and $N = 3$ (triadic wavelets).

1.3. Prediction filters originated from splines

It was mentioned in the introduction (Section 1.1) that once we constructed a spline that interpolates a signal on a sparse grid, we have to predict missing samples of the signal by the values of the spline at the intermediate points. Calculation of

these values reduces to filtering the array of interpolated samples. We derive these filters for different types of splines.

1.3.1. Filters originated from continuous splines

In this section, we use continuous splines as a source for the filter design.

1.3.1.1. B-splines

The centered B-spline of first order is the characteristic function of the interval $[-1/2, 1/2]$. The centered B-spline of order p is the convolution $M^p(x) = M^{p-1}(x) * M^1(x)$, $p \geq 2$. Note that the B-spline of order p is supported on the interval $(-p/2, p/2)$. It is positive within its support and symmetric around zero. The B-spline M^p consists of pieces of polynomials of degree $p-1$ that are linked to each other at the nodes such that $M^p \in C^{p-2}$. Nodes of B-splines of even order are located at points $\{k\}$ and of odd order at points $\{k + 1/2\}$, $k \in \mathbb{Z}$.

The Fourier transform of the B-spline of order p is

$$\widehat{M^p}(\omega) \triangleq \int_{-\infty}^{\infty} e^{-i\omega x} M^p(x)dx = \left(\frac{\sin \omega/2}{\omega/2}\right)^p. \tag{1.22}$$

The time-domain representation of the B-spline is

$$M^p(t) = \frac{1}{(p-1)!} \sum_{k=0}^{p-1} (-1)^k \binom{p}{k} \left(t + \frac{p}{2} - k\right)_+^{p-1}, \tag{1.23}$$

where $t_+ \triangleq (t + |t|)/2$.

We introduce the following sequences:

$$\mathbf{v}_0^p \triangleq \{M^p(k)\}, \qquad \mathbf{v}_{r,N}^p \triangleq \left\{M^p\left(k + \frac{r}{N}\right)\right\}, \quad r \in \mathbb{Z}. \tag{1.24}$$

Their z-transforms are, respectively, $v_0^p(z)$ and $v_{r,N}^p(z)$.

Due to the compact support of B-splines, these sequences are finite and the z-transforms are the Laurent polynomials.

Example 1.2. The Laurent polynomials for splines of second to fourth degrees are as follows.

Linear spline, $p = 2$:

$$v_0^2(z) = 1, \qquad v_{1,2}^2(z) = \frac{z+1}{2}, \qquad v_{1,3}^2(z) = v_{-1,3}^2(z^{-1}) = \frac{z+2}{3}. \tag{1.25}$$

Quadratic spline, $p = 3$:

$$v_0^3(z) = \frac{z + 6 + z^{-1}}{8}, \qquad v_{1,2}^3(z) = \frac{z+1}{2}, \qquad v_{1,3}^3(z) = v_{-1,3}^3(z^{-1}) = \frac{25z + 46 + z^{-1}}{72}. \tag{1.26}$$

Cubic spline, $p = 4$:

$$v_0^4(z) = \frac{z + 4 + z^{-1}}{6}, \qquad v_{1,2}^4(z) = \frac{z^2 + 23z + 23 + z^{-1}}{48}, \qquad v_{1,3}^4(z) = v_{-1,3}^4(z^{-1}) = \frac{z^2 + 60z + 93 + 8z^{-1}}{162}. \tag{1.27}$$

Spline of fourth degree, $p = 5$:

$$v_0^5(z) = \frac{z^2 + 76z + 230 + 76z^{-1} + z^{-2}}{384}, \qquad v_{1,2}^5(z) = \frac{z^2 + 11z + 11 + z^{-1}}{24}, \qquad v_{1,3}^5(z) = v_{-1,3}^5(z^{-1}) = \frac{625z^2 + 11516z + 16566 + 2396z^{-1} + z^{-2}}{31104}. \tag{1.28}$$

Proposition 1.3. *The Laurent polynomials $v_0^p(z)$ and $z^{-r}v_{r,2r}^p(z^{2r})$ are symmetric. The roots of $v_0^p(z)$ are all simple and negative. In addition, for all z, $|z| = 1$, $v_0^p(z) > 0$. All the Laurent polynomials become 1 at $z = 1$.*

1.3.1.2. Interpolatory continuous splines

Shifts of B-splines form a basis in the space of splines of order p on the grid $\{Nl\}_{l\in\mathbb{Z}}$. Namely, any spline S^p has the following representation:

$$S^p(x) = \sum_l q_l M^p\left(\frac{x}{N} - l\right). \tag{1.29}$$

Denote $\mathbf{q} \triangleq \{q_l\}$, $\mathbf{s}_{0,N}^p = \{s_{0,N}^p(l) \triangleq S^p(Nl)\}$, $\mathbf{s}_{r,N}^p = \{s_{r,N}^p(l) \triangleq S^p(Nl + r)\}$, $r \in \mathbb{Z}$, and let $Q(z)$, $s_{0,N}^p(z)$ and $s_{r,N}^p(z)$ be the z-transforms of these the sequences, respectively. We have

$$s_{0,N}^p(l) = \sum_n q_l M^p(l - n) \Longleftrightarrow s_{0,N}^p(z) = Q(z)v_0^p(z). \tag{1.30}$$

Thus, $s_{0,N}^p(z) = Q(z)v_0^p(z)$, where $v_0^p(z)$ is the z-transform of the sequence $\mathbf{u}^p$ defined in (1.24). From these formulas, we can derive expressions for the coefficients of the spline S_i^p which interpolates the given sequence $\mathbf{x}_0 \triangleq \{x_0(l)\} \in l^1$ at grid

points $\{Nl\}_{l\in\mathbb{Z}}$:

$$\begin{aligned} S_i^p(Nl) = x_0(l), \quad & l \in \mathbb{Z}, \\ \Longleftrightarrow\ & Q(z)v_0^p(z) = X_0(z) \\ \Longleftrightarrow\ & Q(z) = \frac{X_0(z)}{v_0^p(z)} \\ \Longleftrightarrow\ & q_l = \sum_{n=-\infty}^{\infty} \lambda_{l-n}^p x_0(n), \end{aligned} \tag{1.31}$$

where $\boldsymbol{\lambda}^p \triangleq \{\lambda_k^p\}$ is the sequence which is defined via its z-transform:

$$\lambda^p(z) = \sum_{k=-\infty}^{\infty} z^{-k}\lambda_k^p = \frac{1}{v_0^p(z)}. \tag{1.32}$$

The coefficients $\{\lambda_k^p\}$ decay exponentially as $|k| \to \infty$. Substitution of (1.31) into (1.29) results in an alternative representation of the interpolatory spline:

$$S_i^p(x) = \sum_{l=-\infty}^{\infty} x_0(l)L^p\left(\frac{x}{N} - l\right), \qquad L^p(x) \triangleq \sum_l \lambda_l^p M^p(x-l). \tag{1.33}$$

The spline $L^p(x)$, defined in (1.33), is called the fundamental spline. It interpolates the Kronecker delta sequence δ_k, that is, it vanishes at all the integer points except $t = 0$, where $L^p(0) = 1$. Due to decay of the coefficients $\{\lambda_k^p\}$, the spline $L^p(t)$ decays exponentially as $|t| \to \infty$.

The values of the fundamental spline at the intermediate points are

$$L^p\left(k + \frac{r}{N}\right) = \sum_l \lambda_l^p M^p\left(k - l + \frac{r}{N}\right), \quad r \in \mathbb{Z}. \tag{1.34}$$

Denote by $V_{r,N}^p(z)$ the z-transform of the sequence $\{L^p(k + r/N)\}$, $k \in \mathbb{Z}$. Then, we obtain from (1.34) that

$$V_{r,N}^p(z) = \frac{v_{r,N}^p(z)}{v_0^p(z)}, \qquad v_{r,N}^p(z) \triangleq \sum_{n\in\mathbb{Z}} z^{-n}M^p\left(n + \frac{r}{N}\right). \tag{1.35}$$

Hence, the values of the interpolatory spline at the intermediate points are

$$s_{r,N}^p(l) = \sum_n L^p\left(l + \frac{r}{N} - n\right)x_0(n) \Longleftrightarrow s_{r,N}^p(z) = V_{r,N}^p(z)X_0(z). \tag{1.36}$$

Switching into the signal processing terminology, we say that in order to derive the values of the interpolatory spline at the points $\{Nl+r\}$ around the points $\{Nl\}$ of interpolation, we have to filter the data $\{x_0(l)\}$ by the filters $V_{r,N}^p$ whose impulse

response $\{L^p(l + r/N)\}$, $k \in \mathbb{Z}$, is finite or decays exponentially as $|l| \to \infty$ (IIR filter).

Let $\mathbf{x} = \{x(l)\}_{l\in\mathbb{Z}}$ and $x_0(l) \triangleq x(Nl)$. Denote $x_r(l) \triangleq x(Nl + r)$. As we mentioned above, if a spline interpolates samples of a signal at $\{Nl\}$, that is, $S_i^p(Nl) = x_0(l)$, then the values of the spline at the points $\{Nl + r\}$ are used as a prediction for the corresponding samples of the signal $\mathbf{x}$: $x_r(l) \approx S_i^p(Nl + r)$.

Definition 1.4. A lowpass filter $F_{r,N}(z)$, whose impulse response $\{f_{r,N}(l)\}_{l\in\mathbb{Z}}$ is finite or decays exponentially, restores polynomials of degree p on the grid $\{Nl + r\}$ if for any polynomial $P(t)$ of degree p, the following identity $\sum_{n\in\mathbb{Z}} f_{r,N}(l - n)P(Nn) = P(Nl + r)$ for all $l \in \mathbb{Z}$ is true.

Example 1.5. The prediction filters derived from the interpolatory splines of second to fourth degrees are as follows.

Linear spline, $p = 2$:

$$V_{1,2}^2(z) = \frac{z+1}{2}, \qquad V_{1,3}^2(z) = V_{-1,3}^2\left(z^{-1}\right) = \frac{z+2}{3}. \tag{1.37}$$

Quadratic spline, $p = 3$:

$$V_{1,2}^3(z) = 4\frac{z+1}{z+6+z^{-1}}, \qquad V_{1,3}^3(z) = V_{-1,3}^3\left(z^{-1}\right) = \frac{25z+46+z^{-1}}{9\left(z+6+z^{-1}\right)}. \tag{1.38}$$

Cubic spline, $p = 4$:

$$V_{1,2}^4(z) = \frac{z^2+23z+23+z^{-1}}{8\left(z+4+z^{-1}\right)}, \qquad V_{1,3}^4(z) = V_{-1,3}^4\left(z^{-1}\right) = \frac{z^2+60z+93+8z^{-1}}{27\left(z+4+z^{-1}\right)}. \tag{1.39}$$

Spline of fourth degree, $p = 5$:

$$\begin{aligned} V_{1,2}^5(z) &= 16\frac{z^2+11z+11+z^{-1}}{z^2+76z+230+76z^{-1}+z^{-2}}, \\ V_{1,3}^5(z) &= V_{-1,3}^5\left(z^{-1}\right) = \frac{625z^2+11516z+16566+2396z^{-1}+z^{-2}}{81\left(z^2+76z+230+76z^{-1}+z^{-2}\right)}. \end{aligned} \tag{1.40}$$

Proposition 1.6 (properties of designed prediction filters). (1) *All filters $V_{r,N}^p(z)$ are lowpass, $V_{r,N}^p(1) = 1$.*

(2) *The filters $V_{r,N}^p(z)$ restore polynomials of degree $p - 1$ on the grid $\{Nl + r\}$.*

(3) *The filters $V_{r,2r}^{2q+1}(z)$, which are derived from splines of odd order (even degree), restore polynomials of degree p on the grid $\{2rl + r\}$ (superconvergence property).*

1.3.2. Filters originated from discrete splines

In this section, we use a special type of the so-called discrete splines as a source for filter design. The discrete splines are defined on the grid $\{k\}$ and they are the counterparts of the continuous polynomial splines.

The signal

$$\mathbf{b}_N^1 = \{b_N^1(l)\} \triangleq \begin{cases} 1 & \text{as } l = 0,\dots,N-1 \\ 0 & \text{otherwise} \end{cases} \Longleftrightarrow B_N^1(z) = 1 + z^{-1} + \cdots + z^{-(N-1)} \tag{1.41}$$

is called the discrete B-spline of first order with length N.

We define by recurrence the higher-order B-splines via discrete convolutions:

$$\mathbf{b}_N^p = \mathbf{b}_N^1 * \mathbf{b}_N^{p-1} \Longleftrightarrow B_N^p(z) = \left(1 + z^{-1} + \cdots + z^{-(N-1)}\right)^p. \tag{1.42}$$

If $N = 2M + 1$ is odd, then we can introduce the so-called centered B-splines as

$$\mathbf{q}_N^p = \{q_N^p(l)\}, \qquad q_N^p(l) \triangleq b_N^p(l + M^p) \Longleftrightarrow Q_N^p(z) = \left(z^M + \cdots + z^{-M}\right)^p. \tag{1.43}$$

In the case when $N = 2M$ is even, centering is possible if the order $p = 2m$ is even. Then,

$$\begin{gathered} \mathbf{q}_N^{2m} = \{q_N^{2m}(l)\}, \\ q_N^{2m}(l) \triangleq b_N^p(l + (2M-1)^m) \Longleftrightarrow Q_N^p(z) = \left(z^{2M-1} + \cdots + z^{-(2M-1)}\right)^m. \end{gathered} \tag{1.44}$$

In both cases, the centered B-splines are symmetric about the point $l = 0$ where they attain their maximal value. We assume that either $N = 2M + 1$ or $N = 2M$ and $p = 2m$.

Similar to continuous splines, the discrete spline $\mathbf{d}_N^p = \{d_N^p(l)\}_{l\in\mathbb{Z}}$ of order p on the grid $\{Nn\}$ is defined as a linear combination with real-valued coefficients of shifts of the centered B-spline:

$$d_N^p(l) \triangleq \sum_{n=-\infty}^{\infty} c_l q_N^p(l - Nn) \Longleftrightarrow D_N^p(z) = C(z^N) Q_N^p(z). \tag{1.45}$$

Let

$$q_{r,N}^p(l) \triangleq q_N^p(r + Nl), \quad r = \begin{cases} -M,\dots,M & \text{if } N = 2M+1, \\ -M+1,\dots,M & \text{if } N = 2M,\ p = 2m, \end{cases} \tag{1.46}$$

be the polyphase components of the discrete B-spline. Then, the polyphase components of the discrete spline are

$$d^p_{r,N}(l) \triangleq \sum_{n=-\infty}^{\infty} c_l q^p_{r,N}(l-N) \Longleftrightarrow D^p_{r,N}(z) = C(z)Q^p_{r,N}(z). \tag{1.47}$$

Proposition 1.7. *The component $Q^p_{0,N}(z)$ is symmetric about inversion $z \to 1/z$ and positive on the unit circle $|z| = 1$. All the components $Q^p_{r,N}(z)$ have the same value at $z = 1$:*

$$Q^p_{r,N}(1) = Q^p_0(1) \quad \forall r. \tag{1.48}$$

Our scheme to design prediction filters, which uses discrete splines, is the same as the scheme that is based on continuous splines. We construct the discrete spline $\mathbf{d}^p_N$, which interpolates even samples of the signal $\mathbf{x}$ on the sparse grid $\{Nl\}$ and predict missing samples by the corresponding values, of the constructed spline. Using (1.47), we find the z-transform of the coefficients of interpolatory spline

$$\begin{aligned} d^p_N(lN) = x(lN) &\Longleftrightarrow D^p_{0,N}(z) \\ &= C(z)Q^p_0(z) = X_{0,N}(z) \Longrightarrow C(z) = \frac{X_{0,N}(z)}{Q^p_{0,N}(z)}. \end{aligned} \tag{1.49}$$

Hence, the polyphase components $\mathbf{d}^p_{r,N}$, which are used for the prediction defined via the z-transforms, are

$$D^p_{r,N}(z) = C(z)Q^p_{r,N}(z) = U^p_{r,N}(z)X_{0,N}(z), \quad U^p_{r,N}(z) \triangleq \frac{Q^p_{r,N}(z)}{Q^p_{0,N}(z)}. \tag{1.50}$$

Thus, in order to predict the missed samples of the signal $\mathbf{x}$, we filter its polyphase component $\mathbf{x}_{0,N}$ with the filters $U^p_{r,N}(z)$. Equation (1.48) implies that $U^p_{r,N}(1) = 1$. Therefore, these filters are lowpass. We focus on filters with the downsampling factors $N = 2$ and $N = 3$.

1.3.2.1. Filters with the downsampling factor $N = 2$: relation to Butterworth filters

In the case when the downsampling factor $N = 2$, the filters $U^{2m}_{1,2}(z)$ can be presented explicitly for any even order $2m$.

We get from (1.44) that

$$Q^{2m}_2(z) = \rho^m(z), \qquad \rho(z) \triangleq z + 2 + \frac{1}{z}. \tag{1.51}$$

Hence, the polyphase components of the B-spline and the prediction filters are

$$Q_{0,2}^{2m}(z^2) = \frac{1}{2}(\rho^m(z) + \rho^m(-z)), \qquad Q_{1,2}^{2m}(z_2) = \frac{z}{2}(\rho^m(z) - \rho^m(-z)),$$
$$U_{1,2}^{2m}(z^2) = z\frac{\rho^m(z) - \rho^m(-z)}{\rho^m(z) + \rho^m(-z)}. \tag{1.52}$$

The filters $U_{1,2}^{2m}(z^2)$ are closely related to Butterworth filters [34], which are widely used in signal processing. To be specific, the functions

$$\lambda^m(z) \triangleq 1 + z^{-1}U_{1,2}^{2m}(z^2) = \frac{2\rho^m(z)}{\rho^m(z) + \rho^m(-z)},$$
$$\chi^m(z) \triangleq 1 - z^{-1}U_{1,2}^{2m}(z^2) = \lambda^m(-z) \tag{1.53}$$

are squared magnitudes of the transfer functions of half-band lowpass and high-pass Butterworth filters of order m, respectively.

1.3.2.2. Filters with downsampling factor $N = 3$

Denote $\tau(z) \triangleq z + 1 + 1/z$, $\theta \triangleq e^{2\pi j/3}$. Then,

$$Q_{0,3}^{p}(z^3) = \frac{\tau^p(z) + \tau^p(z\theta) + \tau^p(z/\theta)}{3},$$
$$Q_{1,3}^{p}(z^3) = z\frac{\tau^p(z) + \tau^p(z\theta)\theta + \tau^p(z/\theta)/\theta}{3}$$
$$\Longrightarrow U_{1,3}^{p}(z^3) = z\frac{\tau^p(z) + \tau^p(z\theta)\theta + \tau^p(z/\theta)/\theta}{\tau^p(z) + \tau^p(z\theta) + \tau^p(z/\theta)}, \tag{1.54}$$
$$Q_{-1,3}^{p}(z^3) = z\frac{\tau^p(z) + \tau^p(z\theta)/\theta + \tau^p(z/\theta)\theta}{3}$$
$$\Longrightarrow U_{1,3}^{p}(z^3) = z\frac{\tau^p(z) + \tau^p(z\theta)/\theta + \tau^p(z/\theta)\theta}{\tau^p(z) + \tau^p(z\theta) + \tau^p(z/\theta)}.$$

1.3.2.3. Examples of prediction filters

Linear discrete splines, $p = 2$:

$$U_{1,2}^{2}(z) = \frac{1+z}{2}, \qquad U_{1,3}^{2}(z) = \frac{2+z}{3}, \qquad U_{-1,3}^{2}(z) = \frac{2+1/z}{3}. \tag{1.55}$$

Quadratic discrete splines, $p = 3$:

$$U_{1,3}^{3}(z) = \frac{3(2+z)}{z+7+1/z}, \qquad U_{-1,3}^{3}(z) = \frac{3(2+1/z)}{z+7+1/z}. \tag{1.56}$$

Cubic discrete splines, $p = 4$:

$$U^4_{1,2}(z) = \frac{4(1+z)}{z+6+1/z}, \qquad U^4_{1,3}(z) = \frac{1/z+16+10z}{4z+19+4/z} = U^4_{-1,3}\left(\frac{1}{z}\right). \tag{1.57}$$

Discrete spline of sixth order, $p = 6$:

$$U^6_{1,2}(z) = \frac{(z+14+z^{-1})(1+z)}{6z^{-1}+20+6z}. \tag{1.58}$$

Discrete spline of eighth order, $r = 4$:

$$U^8_{1,2}(z) = \frac{8(1+z)(z^{-1}+6+z)}{z^{-2}+28z^{-1}+70+28z+z^2}. \tag{1.59}$$

1.4. Biorthogonal wavelet transforms generated by filter banks with downsampling factor $N = 2$ (diadic transforms)

In this section, we describe how to generate families of biorthogonal wavelet transforms and wavelet frames using spline-based prediction filters with downsampling factor $N = 2$ designed in Section 1.3. A useful tool for the design and implementation of the biorthogonal wavelet transforms when downsampling factor $N = 2$ is provided by the so-called lifting scheme introduced by Sweldens [44].

1.4.1. Lifting scheme: decomposition

Generally, the lifting mode of the wavelet transform consists of four steps: (1) split, (2) predict, (3) update or lifting, and (4) normalization.

(1) *Split*. The signal $\mathbf{x} = \{x(l)\}_{l\in\mathbb{Z}}$ is split into its polyphase components: $\mathbf{x}_r = \{x_r(l) \triangleq x(2l+r)\}_{l\in\mathbb{Z}}$, $r = 0, 1$.

(2) *Predict*. The even polyphase component is filtered by some lowpass prediction filter $\widetilde{F}(1/z)$, in order for the filtered version of $\mathbf{x}_0$ to predict the odd component $\mathbf{x}_1$. Then, the existing array $\mathbf{x}_1$ is replaced by the array $\mathbf{a}^1$, which is the difference between $\mathbf{x}_1$ and the predicted array.

In the z-domain, the operations are described as $\widetilde{A}^1(z) = X_1(z) - \widetilde{F}(1/z)X_0(z)$.

(3) *Update (lifting)*. Generally, downsampling the original signal $\mathbf{x}$ into $\mathbf{x}_0$ depletes the smoothness of the signal. To obtain a sparse signal similar to the original $\mathbf{x}$, the new odd array is filtered by a lowpass *update* filter, which we prefer to denote as $F(z)/2$. The filtered array is used to increase the smoothness of the even array $\mathbf{x}_0$:

$$\widetilde{A}^0(z) = X_0(z) + \frac{1}{2}F(z)\widetilde{A}^1(z). \tag{1.60}$$

Provided that the filter F is properly chosen, the even array $\mathbf{x}_0$ is transformed into a smoothed and downsampled replica of $\mathbf{x}$.

(4) *Normalization*. Finally, the smoothed array $\widetilde{\mathbf{y}}^0$ and the array of details $\widetilde{\mathbf{y}}^1$ are obtained by the operations $\widetilde{\mathbf{y}}^0 = \sqrt{2}\widetilde{\mathbf{a}}^0$, $\widetilde{\mathbf{y}}^1 = \widetilde{\mathbf{a}}^1/\sqrt{2}$.

1.4.2. Lifting scheme: reconstruction

One of the most attractive features of lifting schemes is that the reconstruction of the signal $\mathbf{x}$ from the arrays $\widetilde{\mathbf{y}}^{\mathbf{0}}$ and $\widetilde{\mathbf{y}}^{\mathbf{1}}$ is implemented by reverse decomposition.

Undo normalization: $\widetilde{\mathbf{a}}^0 = \widetilde{\mathbf{y}}^0/\sqrt{2}\ \widetilde{\mathbf{a}}^1 = \sqrt{2}\widetilde{\mathbf{y}}^1$.

Undo lifting: the even polyphase component $X_0(z) = \widetilde{A}^0(z) - (1/2)F(z)\widetilde{A}^1(z)$ is restored.

Undo predict: the odd polyphase component

$$X_1(z) = \widetilde{A}^1(z) + \widetilde{F}\left(\frac{1}{z}\right)X_0(z) \tag{1.61}$$

is restored.

Undo split: the last step is the standard restoration of the signal from its even and odd components. In the z-domain, it appears as $X(z) = X_1(z^2) + z^{-1}X_0(z^2)$.

1.4.3. Filter banks

Rewriting the lifting steps in a matrix form, we obtain the polyphase matrices of the wavelet transforms to be

$$\begin{pmatrix}\widetilde{Y}^0(z)\\ \widetilde{Y}^1(z)\end{pmatrix} = \begin{pmatrix}\sqrt{2} & 0\\ 0 & \dfrac{1}{\sqrt{2}}\end{pmatrix}\cdot\begin{pmatrix}1 & \dfrac{F(z)}{2}\\ 0 & 1\end{pmatrix}\cdot\begin{pmatrix}1 & 0\\ -\widetilde{F}\left(\dfrac{1}{z}\right) & 1\end{pmatrix}\cdot\begin{pmatrix}X_0(z)\\ X_1(z)\end{pmatrix}. \tag{1.62}$$

Hence, the analysis polyphase matrix is

$$\widetilde{\mathbf{P}}\left(\frac{1}{z}\right) = \begin{pmatrix}\sqrt{2}\left(1 - \dfrac{\widetilde{F}(1/z)F(z)}{2}\right) & \dfrac{F(z)}{\sqrt{2}}\\ -\dfrac{\widetilde{F}(1/z)}{\sqrt{2}} & \dfrac{1}{\sqrt{2}}\end{pmatrix}. \tag{1.63}$$

The reconstruction operations are represented by

$$\begin{pmatrix}X_0(z)\\ X_1(z)\end{pmatrix} = \begin{pmatrix}1 & 0\\ \widetilde{F}\left(\dfrac{1}{z}\right) & 1\end{pmatrix}\cdot\begin{pmatrix}1 & \dfrac{-F(z)}{2}\\ 0 & 1\end{pmatrix}\cdot\begin{pmatrix}\dfrac{1}{\sqrt{2}} & 0\\ 0 & \sqrt{2}\end{pmatrix}\cdot\begin{pmatrix}\widetilde{Y}^0(z)\\ \widetilde{Y}^1(z)\end{pmatrix}. \tag{1.64}$$

Hence, the synthesis polyphase matrix is

$$\mathbf{P}(z) = \begin{pmatrix} \dfrac{1}{\sqrt{2}} & \dfrac{-F(z)}{\sqrt{2}} \\ \dfrac{\widetilde{F}(1/z)}{\sqrt{2}} & \sqrt{2}\left(1 - \dfrac{\widetilde{F}(1/z)F(z)}{2}\right) \end{pmatrix}. \tag{1.65}$$

Obviously, $\mathbf{P}(z) = \widetilde{\mathbf{P}}(1/z)^{-1}$. Therefore, the perfect reconstruction condition is satisfied. We recall that

$$\widetilde{\mathbf{P}}(z) \triangleq \begin{pmatrix} \widetilde{H}_0^0(z) & \widetilde{H}_1^0(z) \\ \widetilde{H}_0^1(z) & \widetilde{H}_1^1(z) \end{pmatrix}, \qquad \mathbf{P}(z) \triangleq \begin{pmatrix} H_0^0(z) & H_0^1(z) \\ H_1^0(z) & H_1^1(z) \end{pmatrix}. \tag{1.66}$$

Thus, the analysis filters are

$$\begin{aligned} \widetilde{H}^0\left(\frac{1}{z}\right) &= \sqrt{2}\left(1 - \frac{\widetilde{F}(z^{-2})F(z^2) - zF(z^2)}{2}\right) = \frac{\sqrt{2}}{2}(1 + zF(z^2) + W(z^2)), \\ \widetilde{H}^1\left(\frac{1}{z}\right) &= z\frac{\sqrt{2}}{2}(1 - z^{-1}\widetilde{F}(z^{-2})), \end{aligned} \tag{1.67}$$

where

$$W(z) \triangleq 1 - \widetilde{F}(z^{-1})F(z). \tag{1.68}$$

Thus, the synthesis filters are

$$\begin{aligned} H^0(z) &= \frac{\sqrt{2}}{2}(1 + z^{-1}\widetilde{F}(z^{-2})) = z^{-1}\widetilde{H}^1\left(\frac{-1}{z}\right), \\ H^1(z) &= z\frac{\sqrt{2}}{2}(1 - z^{-1}F(z^{-2}) + W(z^2)). \end{aligned} \tag{1.69}$$

If one polyphase component of the filter $H(z)$ is a constant number, then the filter is called interpolatory. We see from (1.69) that the lowpass synthesis filter $H^0(z)$ is interpolatory. Consequently, the synthesis scaling function $\varphi(t)$, which is generated by $H^0(z)$, interpolates the Kroneker delta (up to a constant c). It means that

$$\varphi(l) = \begin{cases} c & \text{if } l = 0, \\ 0 & \text{otherwise,} \end{cases} \qquad l \in \mathbb{Z}. \tag{1.70}$$

1.4.4. Wavelets derived from spline-based filter banks

The perfect reconstruction condition for the presented filter banks is satisfied with any choice of lowpass filters $\widetilde{F}(z)$ and $F(z)$. However, once the filters $V_{1,2}^p(z)$ and

$U_{1,2}^{2m}(z)$, derived from continuous and discrete splines, respectively, are utilized, a diverse family of biorthogonal wavelets appears. Properties of these wavelets such as symmetry, interpolation, smoothness, flat spectra, good time-domain localizations, and vanishing moments fit well signal processing needs. Implementation of these transforms is highly efficient.

Note that number of vanishing moments in the *analysis* wavelets is important for the applications of signal processing while typical requirements to the *synthesis* wavelets are smoothness and good time-domain localization.

Proposition 1.8. *If any of the filters $V_{1,2}^{p}(z)$ and $U_{1,2}^{2m}(z)$ derived from splines is used as the prediction filter $\widetilde{F}(1/z)$ and any of them is used as the update filter $F(z)$, then*

(1) *the filters $\widetilde{H}^0$ and H^0 are lowpass while the filters $\widetilde{H}^1$ and H^1 are highpass;*

(2) *the filters $\widetilde{H}^0$ and H^0 generate continuous scaling functions $\widetilde{\varphi}(t)$ and $\varphi(t)$, whereas the filters $\widetilde{H}^1$ and H^1 generate continuous wavelets $\widetilde{\psi}(t)$ and $\psi(t)$ with vanishing moments;*

(3) *the filters in the analysis and synthesis filter banks are symmetric (up to a shift) about inversion $z \to 1/z$ and corresponding waveforms are symmetric in time domain and decay exponentially as $t \to \infty$.*

Update filters: in principle, any lowpass filter can serve as the update filter $F(z)$. However, in what follows, we choose the update filter $F(z)$ to be equal to the predict filter $\widetilde{F}(z)$.

1.4.5. Continuous splines

Proposition 1.9. *If the prediction filter in the lifting scheme $F(1/z) = V_{1,2}^{2m}(z)$ is derived from the continuous spline of even order $2m$, then*

(1) *the transfer function of the analysis highpass filter $\widetilde{H}^1(z)$ has zero of multiplicity $2m$ at $z = 1$, consequently, the analysis wavelet $\widetilde{\psi}(t)$ has $2m$ vanishing moments;*

(2) *the synthesis scaling function $\varphi(t)$ is equal to the fundamental spline $L^{2m}(x)$ of order $2m$ defined in* (1.33)*, consequently, it is continuous together with its derivatives up to order $2m-2$ (belongs to C^{2m-2});*

(3) *the synthesis wavelet $\psi(t)$ is a spline of order $2m$, and therefore, belongs to C^{2m-2}.*

Proposition 1.10. *If the prediction filter in the lifting scheme $F(1/z) = V_{1,2}^{2m-1}(z)$ is derived from the continuous spline of odd order $2m-1$, then*

(1) *the transfer function of the analysis highpass filter $\widetilde{H}^1(z)$ has zero of multiplicity $2m$ at $z = 1$, consequently, the analysis wavelet $\widetilde{\psi}(t)$ has $2m$ vanishing moments;*

(2) *the synthesis scaling function $\varphi(t)$ and the wavelet $\psi(t)$ are smoother than the generating spline (which belongs to C^{2m-3}).*

Example 1.11

Linear spline, $p = 2$:

$$\begin{aligned}\widetilde{H}^1(z) &= \frac{z\left(1 - z^{-1}V_{1,2}^2(z^2)\right)}{\sqrt{2}} = -\frac{(1-z)^2}{2\sqrt{2}},\\ H^0(z) &= z^{-1}\widetilde{H}^1(-z) = \frac{z^{-1}+2+z}{2\sqrt{2}}.\end{aligned} \tag{1.71}$$

The corresponding analysis wavelet $\widetilde{\psi}(t)$ has two vanishing moments. The synthesis waveforms belong to C^0.

Quadratic spline, $p = 3$:

$$\widetilde{H}^1(z) = z^{-1}\frac{(1-z)^4}{\sqrt{2}(z^2+6+z^{-2})}, \qquad H^0(z) = \frac{\left(z^{-1}+2+z\right)^2}{\sqrt{2}(z^2+6+z^{-2})}. \tag{1.72}$$

The corresponding analysis wavelet $\widetilde{\psi}(t)$ has four vanishing moments. The synthesis waveforms belong to C^2.

Cubic spline, $p = 4$:

$$\widetilde{H}^1(z) = z^{-1}\frac{(1-z)^4\left(z+4+z^{-1}\right)}{8\sqrt{2}(z^{-2}+4+z^2)}, \qquad H^0(z) = \frac{\left(z^{-1}+2+z\right)^2\left(z+4+z^{-1}\right)}{8\sqrt{2}(z^{-2}+4+z^2)}. \tag{1.73}$$

The corresponding analysis wavelet $\widetilde{\psi}(t)$ has four vanishing moments. The synthesis waveforms belong to C^2.

Interpolatory spline of fourth degree, $p = 5$:

$$\begin{aligned}\widetilde{H}^1(z) &= -z^{-2}\frac{(1-z)^6\left(z+z^{-1}-10\right)}{\sqrt{2}\left(z^4+76z^2+230+76z^{-2}+z^{-4}\right)},\\ H^0(z) &= \frac{\left(z+2+z^{-1}\right)^3\left(z+z^{-1}+10\right)}{\sqrt{2}\left(z^4+76z^2+230+76z^{-2}+z^{-4}\right)}.\end{aligned} \tag{1.74}$$

The corresponding analysis wavelet $\widetilde{\psi}(t)$ has six vanishing moments. The synthesis waveforms belong to C^4.

We display in Figures 1.1–1.4 the frequency responses of the analysis and synthesis filter banks, which are derived from continuous splines, and the corresponding scaling functions and wavelets. All the figures are organized identically. Each figure consists of four columns. The first column from left displays the analysis scaling function $\widetilde{\varphi}(t)$ (bottom) and the analysis wavelet $\widetilde{\psi}(t)$ (top). The second column from left displays the frequency responses of the analysis lowpass filter $\widetilde{H}^0(z)$ (bottom) and the analysis highpass filter $\widetilde{H}^1(z)$ (top). Next column displays

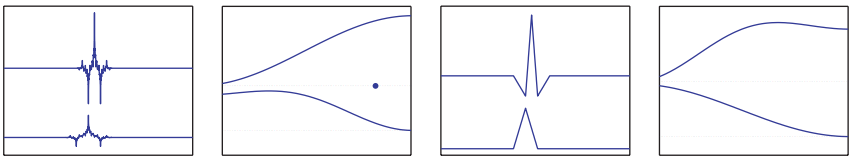

FIGURE 1.1. Filters and wavelets derived from the linear continuous spline.

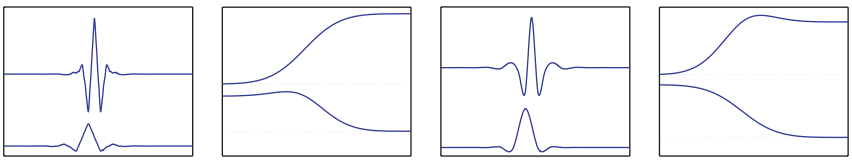

FIGURE 1.2. Filters and wavelets derived from the quadratic continuous spline.

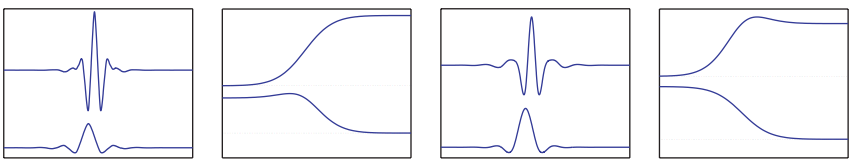

FIGURE 1.3. Filters and wavelets derived from the cubic continuous spline.

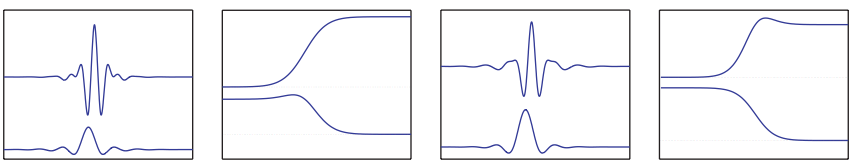

FIGURE 1.4. Filters and wavelets derived from the continuous spline of fourth degree.

the synthesis scaling function $\varphi(t)$ (bottom) and the synthesis wavelet $\psi(t)$ (top). Last column displays the frequency responses of the synthesis lowpass filter $H^0(z)$ (bottom) and the synthesis highpass filter $H^1(z)$ (top).

1.4.6. Discrete splines

Proposition 1.12. *If the prediction filter in the lifting scheme* $F(1/z) = U_{1,2}^{2m}(z)$ *is derived from the discrete spline of even order* $2m$*, then*

(1) *the transfer function of the analysis highpass filter* $\widetilde{H}^1(z)$ *has zero of multiplicity* $2m$ *at* $z = 1$*, consequently, the analysis wavelet* $\widetilde{\psi}(t)$ *has* $2m$ *vanishing moments;*

(2) *the transfer function of the synthesis lowpass filter* $H^0(z)$ *and the analysis highpass filter* $z^{-1}\widetilde{H}^1(z)$ *are the squared magnitudes of the transfer functions of half-band lowpass and highpass Butterworth filters of order* m*, respectively.*

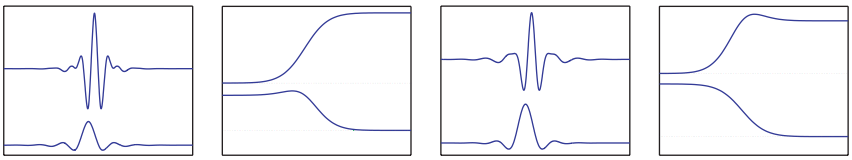

FIGURE 1.5. Filters and wavelets derived from the discrete spline of fifth degree.

Example 1.13

Linear spline, $m = 1$: the filter bank coincides with the filter bank derived from the continuous linear spline.

Cubic spline, $m = 2$: the filter bank coincides with the filter bank derived from the continuous quadratic spline.

Discrete spline of fifth degree, $m = 3$:

$$\widetilde{H}^1(z) = z^{-2}\frac{(1-z)^6}{\sqrt{2}\left(6z^2+20+6z^{-2}\right)}, \qquad H^0(z) = -\frac{\left(z^{-1}-2+z\right)^3}{\sqrt{2}\left(6z^2+20+6z^{-2}\right)}. \tag{1.75}$$

The corresponding analysis wavelet $\widetilde{\psi}(t)$ has six vanishing moments. The synthesis waveforms belong to C^4.

Discrete spline of seventh degree, $m = 4$:

$$\widetilde{H}^1(z) = z^{-3}\frac{(1-z)^8}{\sqrt{2}\left(z^{-4}+28z^{-2}+70+28z^2+z^4\right)}, \qquad H^0(z) = \frac{\left(z^{-1}-2+z\right)^4}{\sqrt{2}\left(z^{-4}+28z^{-2}+70+28z^2+z^4\right)}. \tag{1.76}$$

The corresponding analysis wavelet $\widetilde{\psi}(t)$ has eight vanishing moments. The synthesis waveforms belong to C^5.

We display in Figures 1.5 and 1.6 the frequency responses of the analysis and synthesis filter banks, which are derived from discrete splines, and the corresponding scaling functions and wavelets. The figures are organized similarly to Figures 1.1–1.4.

Remarks 1.14. (1) From the above figures, we see that the designed waveforms are smooth (except for the analysis waveforms derived from the linear spline), well localized in time domain, and symmetric.

(2) The frequency responses of filters are maximally flat (has no ripples) in the passband, and rolls towards zero in the stopband. As the order of the generating spline is high, the decline is steeper in the stopband.

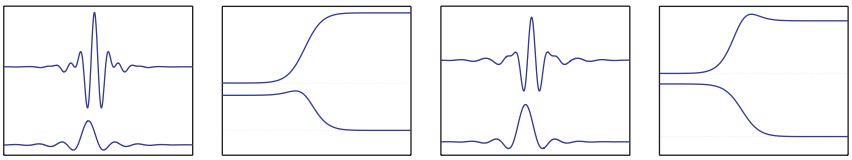

FIGURE 1.6. Filters and wavelets derived from the discrete spline of seventh degree.

(3) The frequency responses of the filters $H^0(z)$ and $\widetilde{H}^1(z)$ are monotonous, whereas the responses of $\widetilde{H}^0(z)$ and $H^1(z)$ have a bump near the cutoff. This bump stems from the presence of the term $W(z)$ in the transfer functions of these filters (see (1.67)–(1.69)). Also, from this reason, the analysis waveforms are less regular than the synthesis counterparts.

(4) The transfer functions of all the designed filters are rational functions. Therefore, the filters (except the filters derived from the linear spline) have infinite impulse response (IIR). But they can be efficiently implemented via causal-anticausal recursive filtering (see the appendix). The computational cost is even lower than the cost of implementing finite impulse response (FIR) filters with similar properties.

Properties of the designed wavelets and filters make them useful for signal processing applications. We describe one application in Section 1.5.

1.5. Application of spline-based wavelet transforms to image compression

The above transforms were applied to multimedia still images to achieve high-quality compression. In most experiments, they outperform the popular B9/7 biorthogonal transform [15, 31], which is the core of JPEG 2000 still image compression standard. In this section, we present the results after compression and decompression of four images in Figures 1.7 and 1.8. These are 512×512 8-bit per pixel (8 bpp) images.

The following experiments were done.

(1) The image was decomposed up to 6 scales by the wavelet transform using the B9/7 transforms and the transforms designed in Section 1.4.

(2) The transform coefficients were coded using the SPIHT algorithm (see [41]) followed by arithmetic coding. This algorithm enables to achieve exact predetermined compression rate. We coded the coefficients with different compression ratios (CR) 1 : 10 (0.8 bpp), 1 : 20 (0.4 bpp), 1 : 30 (4/15 bpp), 1 : 40 (0.2 bpp), and 1 : 50 (4/25 bpp).

(3) The reconstructed image was compared with the original image and the achieved peak signal-to-noise ratio (PSNR) in decibels was computed:

$$\mathrm{PSNR} = 10 \log_{10} \left(\frac{N 255^2}{\sum_{k=1}^{N} \left(x(k) - \widetilde{x}(k) \right)^2} \right) \mathrm{dB}. \tag{1.77}$$

(a) (b)

FIGURE 1.7. (a) Lena, (b) Barbara.

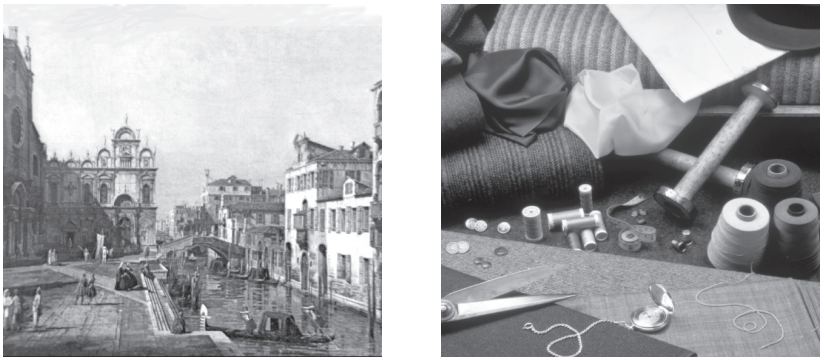

(a) (b)

FIGURE 1.8. (a) Canaletto, (b) fabrics.

We denote the transforms as follows.

(i) B9/7 denotes the B9/7 biorthogonal transform.
(ii) CS3 denotes the transform generated by quadratic continuous spline (1.72).
(iii) CS4 denotes the transform generated by cubic continuous spline (1.73).
(iv) CS5 denotes the transform generated by continuous spline of fourth degree (1.74).
(v) DS3 denotes the transform generated by discrete spline of sixth degree (1.75).
(vi) DS4 denotes the transform generated by discrete spline of eighth degree (1.76).

The results are summarized in Tables 1.1–1.4.

Lena: the PSNR values of "Lena" are presented in Table 1.1.

All the spline wavelet transforms outperform the B9/7 filter in any compression rate (with one exception for CS3 at CR = 10). In Figure 1.9, we display the

TABLE 1.1. PSNR of "Lena" after the application of SPIHT where the decomposition of the wavelet transform was 6 scales.

CR	B9/7	CS3	CS4	CS5	DS3	DS4
10	39.12	39.09	39.14	**39.15**	**39.15**	39.14
20	36.08	36.14	36.17	36.17	**36.18**	36.12
30	34.12	34.23	34.27	34.29	**34.30**	34.23
40	32.99	33.05	33.08	33.07	**33.09**	33.08
50	31.90	31.91	**31.98**	31.96	**31.98**	31.92

TABLE 1.2. PSNR of "Barbara" after the application of SPIHT where the decomposition of the wavelet transform was 6 scales.

CR	B9/7	CS3	CS4	CS5	DS3	DS4
10	35.36	35.64	35.99	36.27	36.21	**36.39**
20	30.63	30.87	31.05	31.19	31.17	**31.27**
30	28.27	28.09	28.27	28.46	28.42	**28.59**
40	26.91	26.78	26.93	27.13	27.08	**27.22**
50	26.17	25.72	25.89	26.04	26.02	**26.18**

TABLE 1.3. PSNR of "Canaletto" after the application of SPIHT where the decomposition of the wavelet transform was 6 scales.

CR	B9/7	CS3	CS4	CS5	DS3	DS4
10	35.10	35.16	35.20	**35.21**	**35.21**	**35.21**
20	31.48	31.59	31.66	**31.68**	**31.68**	31.67
30	29.54	29.66	29.71	**29.74**	**29.74**	29.72
40	28.38	28.50	28.54	28.54	**28.55**	28.52
50	27.55	27.63	**27.63**	**27.63**	**27.63**	27.62

TABLE 1.4. PSNR of "fabrics" after the application of SPIHT where the decomposition of the wavelet transform was 6 scales.

CR	B9/7	CS3	CS4	CS5	DS3	DS4
10	**36.30**	36.21	36.24	36.24	36.24	36.20
20	**32.58**	32.42	32.45	32.45	32.45	32.43
30	**31.14**	31.02	31.07	31.04	31.06	30.99
40	**30.08**	30.04	30.03	30.03	30.03	29.97
50	**29.38**	29.36	29.37	29.36	29.37	29.31

closed-up fragments of "Lena" reconstructed from 1 : 50 compression files of wavelet coefficients of the B9/7 and DS3 transforms.

Barbara: the PSNR values of "Barbara" are presented in Table 1.2.

All the spline-wavelet transforms outperform the B9/7 filter in any compression rate, especially at high bit rate. Most efficient is the DS4, where the wavelets have eight vanishing moments and the synthesis waveforms belong to C^4. In Figure 1.10, we display closed-up fragments of "Barbara" reconstructed from 1 : 40 compression files of wavelet coefficients of B9/7 and DS4 transforms.

Canaletto: the PSNR values of "Canaletto" are presented in Table 1.3.

(a) (b)

FIGURE 1.9. Reconstruction of "Lena" from 1 : 50 compression files of wavelet coefficients of B9/7 (a) and DS3 (b) transforms.

(a) (b)

FIGURE 1.10. Reconstruction of "Barbara" from 1 : 50 compression files of wavelet coefficients of B9/7 (a) and DS4 (b) transforms.

All the splinetransforms slightly outperform the B9/7 filter in any compression rate. Most efficient are the DS3 and DS4, where the wavelets have six and eight vanishing moments, respectively. In Figure 1.11, we display closed-up fragments of "Canaletto" reconstructed from 1 : 40 compression files of wavelet coefficients of B9/7 and DS3 transforms.

Fabrics: the PSNR values of "fabrics" are presented in Table 1.4.

The B9/7 filter demonstrates a small advantage of the PSNR over all splinetransforms on this image. In Figure 1.12, we display closed-up fragments of "fabrics" reconstructed from 1 : 50 compression files of wavelet coefficients of B9/7 and DS3 transforms.

The examples presented above demonstrate that the performance of the designed spline-based wavelet transforms for image compression is competitive to the performance of the popular B9/7 transform, which is used in JPEG 2000. Once

(a) (b)

FIGURE 1.11. Reconstruction of "Canaletto" from 1 : 50 compression files of wavelet coefficients of B9/7 (a) and DS3 (b) transforms.

(a) (b)

FIGURE 1.12. Reconstruction of "fabrics" from 1 : 50 compression files of wavelet coefficients of B9/7 (a) and DS3 (b) transforms.

the recursive implementation of the spline filters is conducted, its computational cost is comparable with the cost of the implementation of B9/7 transform. For example, the number of additions (A) and multiplications (M) per pixel for the B9/7 transform is 8A + 4M, whereas for the transform CS3, it is 8A + 6M operations. The efficient DS3 transform requires 12A + 8M operations.

1.6. Wavelet frames (framelets) generated by 3-channel filter banks with downsampling factor $N = 2$

As we mentioned in the end of Section 1.4, the analysis wavelets are less regular than the synthesis ones. The reason is that the structure of the lowpass analysis filters is more complicated than the structure of their synthesis counterparts. The latter is very simple and has the interpolation property. If the prediction filter originates from the discrete spline, then the lowpass synthesis filter coincides with the

squared magnitude of the transfer function of half-band lowpass Butterworth filter. Also we mentioned the bumps that disturbed the flatness of the frequency responses of the lowpass analysis filters and the highpass synthesis ones. We can essentially improve the properties of the filters and waveforms by introducing additional channel into the filter bank retaining the perfect reconstruction property. Thus, the representation of a signal becomes redundant and produces a frame expansions of signals. The redundancy should hardly be regarded as a drawback. The redundant representations have more adaptation abilities compared to basis expansions of signals. Therefore, they are feasible for signal denoising and features extraction. This redundancy enables to exploit frame expansion as a tool for recovery of erasures, which may occur while a multimedia signal is transmitted through a lossy channel.

1.6.1. Interpolatory frames

In this section, we describe how to construct frames in signal space starting from either any pair of lowpass interpolatory filters or from a single filter. The problem reduces to the design of a perfect reconstruction filter bank with desired properties. The key point in this design is the factorization scheme of a polyphase matrix.

We introduce an analysis-synthesis pair of lowpass interpolatory filters

$$\widetilde{G}^0(z) \triangleq \frac{\sqrt{2}}{2}\left(1 + z^{-1}\widetilde{F}(z^2)\right), \qquad G^0(z) \triangleq \frac{\sqrt{2}}{2}\left(1 + z^{-1}F(z^2)\right), \tag{1.78}$$

that are similar to the lowpass interpolatory synthesis filter $H^0(z)$ derived from the lifting scheme (see (1.69)). As before, denote $W(z) \triangleq 1 - F(z)\widetilde{F}(z^{-1})$.

The polyphase matrices for the filter banks $\widetilde{G}^0$, $\widetilde{G}^1$, $\widetilde{G}^2$ and G^0, G^1, G^2 comprising the interpolatory lowpass filters $G^0(z)$ and $\widetilde{G}^0(z)$ are

$$\widetilde{\mathbf{P}}(z) \triangleq \begin{pmatrix} \dfrac{1}{\sqrt{2}} & \dfrac{\widetilde{F}(z)}{\sqrt{2}} \\ \widetilde{G}_0^1(z) & \widetilde{G}_1^1(z) \\ \widetilde{G}_0^2(z) & \widetilde{G}_1^2(z) \end{pmatrix}, \qquad \mathbf{P}(z) \triangleq \begin{pmatrix} \dfrac{1}{\sqrt{2}} & G_0^1(z) & G_0^2(z) \\ \dfrac{F(z)}{\sqrt{2}} & G_1^1(z) & G_1^2(z) \end{pmatrix}. \tag{1.79}$$

Then, the perfect reconstruction condition (1.12) leads to

$$\mathbf{P}_g(z) \cdot \widetilde{\mathbf{P}}_g\left(\frac{1}{z}\right) = \frac{1}{2}\mathbf{Q}(z), \tag{1.80}$$

where

$$\widetilde{\mathbf{P}}_g(z) \triangleq \begin{pmatrix} \widetilde{G}_0^1(z) & \widetilde{G}_1^1(z) \\ \widetilde{G}_0^2(z) & \widetilde{G}_1^2(z) \end{pmatrix}, \qquad \mathbf{P}_g(z) \triangleq \begin{pmatrix} G_0^1(z) & G_0^2(z) \\ G_1^1(z) & G_1^2(z) \end{pmatrix},$$
$$\mathbf{Q}(z) \triangleq \begin{pmatrix} 1 & -\widetilde{F}(z^{-1}) \\ -F(z) & 2 - F(z)\widetilde{F}(z^{-1}) \end{pmatrix}. \tag{1.81}$$

Therefore, the construction of a frame with the interpolatory lowpass filters $\widetilde{G}^0(z)$ and $G^0(z)$ reduces to factorization of the matrix $\mathbf{Q}(z)$ as in (1.80). There are many options for this factorization of $\mathbf{Q}(z)$. We describe implications of the simplest triangular factorization:

$$\widetilde{\mathbf{P}}_g(z) = \frac{1}{\sqrt{2}} \begin{pmatrix} 0 & \widetilde{w}(z) \\ 1 & -\widetilde{F}(z) \end{pmatrix}, \quad \mathbf{P}_g(z) = \frac{1}{\sqrt{2}} \begin{pmatrix} 0 & 1 \\ w(z) & -F(z) \end{pmatrix}, \quad w(z)\widetilde{w}(z^{-1}) = W(z). \tag{1.82}$$

Thus, to complete the construction, we have to factorize the function $W(z)$. As soon as it is done, we obtain the perfect reconstruction filter bank,

$$\begin{aligned} \widetilde{G}^0(z) &\triangleq \frac{\sqrt{2}}{2}(1 + z^{-1}\widetilde{F}(z^2)), & G^0(z) &\triangleq \frac{\sqrt{2}}{2}(1 + z^{-1}F(z^2)), \\ \widetilde{G}^1(z) &= \frac{z^{-1}\widetilde{w}(z^2)}{\sqrt{2}}, & G^1(z) &= \frac{z^{-1}w(z^2)}{\sqrt{2}}, \\ \widetilde{G}^2(z) &= \frac{1 - z^{-1}\widetilde{F}(z^2)}{\sqrt{2}} = \widetilde{H}(-z), & G^2(z) &= \frac{1 - z^{-1}F(z^2)}{\sqrt{2}} = H(-z). \end{aligned} \tag{1.83}$$

Note that in this case, the filters $G^2(z)$ and $\widetilde{G}^2(z)$ are interpolatory. If $F(1) = \widetilde{F}(1)$, then these filters are highpass. The filters $\widetilde{G}^1(z)$ and $G^1(z)$ have no even polyphase component.

This filter bank generates a biframe in signal space.

We use, as the prediction filters $\widetilde{F}(z)$ and $F(z)$, the spline-based filters $V_{1,2}^p(z)$ and $U_{1,2}^{2m}(z)$, which are designed in Section 1.3. All these filters possess the symmetry property: $z^{-1}F(z^2) = zF(z^{-2})$. Thus, the filters $\widetilde{G}^0(z)$, $\widetilde{G}^2(z)$, $G^0(z)$, and $G^2(z)$ are symmetric about inversion $z \to 1/z$. The rational function $W(z^2)$ can be written as $W(z^2) = (1 - z^{-1}F(z^2) \cdot z\widetilde{F}(z^{-2}))/2 = W(z^{-2})$. Thus, a rational symmetric or antisymmetric factorization is possible. The trivial rational symmetric factorizations are $\nu(z) = 1$, $\widetilde{\nu}(z) = W(z)$ or $\widetilde{\nu}(z) = 1$, $\nu(z) = W(z)$. Since $W(z^2) = 0$ if $z = \pm 1$, at least one of the filters $G^2(z)$ and $\widetilde{G}^2(z)$ is bandpass and the corresponding framelet has vanishing moments.

1.6.2. Tight and semitight frames

If $F(z) = \widetilde{F}(z)$, then we get $G^0(z) = \widetilde{G}^0(z)$, $G^2(z) = \widetilde{G}^2(z)$, and

$$W(z) = \frac{1 - |F(z)|^2}{2}, \qquad W(z^2) = 2G^0(z)G^0(-z). \tag{1.84}$$

If the inequality

$$|F(z)| \le 1, \quad \text{as } |z| = 1, \tag{1.85}$$

holds, then the function $W(z)$ can be factorized as $W(z) = w(z)w(1/z)$. This factorization is not unique. Due to Riesz's lemma [19], a rational factorization is possible. Then, we have $G^1(z) = \widetilde{G}^1(z)$. Thus, the synthesis filter bank coincides with the analysis filter bank and generates a tight frame. Due to (1.84), the (anti)symmetric rational factorization is possible if and only if all roots and poles of the function $G^0(z)$ have even multiplicity. If $G^0(z)$ has a root of multiplicity $2m$ at $z = 1$, then the filter $G^1(z)$ has roots of multiplicity m at $z = 1$ and $z = -1$. The corresponding framelet $\psi^1(t)$ has m vanishing moments. A similar construction for the tight frame based on a family of interpolatory symmetric FIR filters was presented in [14]. However, the filter $G^1(z)$ in [14] lacks symmetry.

If the condition (1.85) is not satisfied, we are still able to generate frames, which are very close to a tight frame. Namely,

$$\begin{aligned} G^0(z)(z) = \widetilde{G}^0(z)(z) &= \frac{1 + z^{-1}F(z^2)}{\sqrt{2}}, \\ G^2(z) = \widetilde{G}^2(z) &= \frac{1 - z^{-1}F(z^2)}{\sqrt{2}}, \\ G^1(z) = \frac{z^{-1}w(z^2)}{\sqrt{2}}, \qquad \widetilde{G}^1(z) &= \frac{z^{-1}\widetilde{w}(z^2)}{\sqrt{2}}, \\ w(z)\widetilde{w}\left(\frac{1}{z}\right) = W(z) &= \left(1 - |F(z)|^2\right). \end{aligned} \tag{1.86}$$

It is natural to refer to such a frame as a *semitight* frame. Due to the symmetry of $W(z)$, an (anti)symmetric factorization of type (1.86) is always possible. Therefore, even when (1.85) holds, sometimes it is preferable to construct a semitight rather than a tight frame. For example, it was proved in [38] that a compactly supported interpolatory symmetric tight frame with two framelets is possible only with the lowpass filter $G^0(z) = (1 + (z + 1/z)/2)/\sqrt{2}$. In this case, the scaling function and the framelets are piecewise linear. The framelets $\psi^2(t)$ and $\psi^1(t)$ have two and one vanishing moments, respectively. However, it is possible to construct a variety of compactly supported interpolatory symmetric semitight frames with smooth framelets. The construction of compactly supported interpolatory symmetric tight frame with three framelets is always possible [14]. On the other hand, in the semitight frames, we can swap vanishing moments between the analysis and

synthesis framelets. Typically, it is advisable to have more vanishing moments in the analysis framelets.

Note that smoothness of all waveforms in a tight or semitight frame is the same.

1.6.3. Tight and semitight frames generated by spline-based filter banks

1.6.3.1. Butterworth frames

If we use as the prediction filters $F(z)$, the filters $U_{1,2}^{2m}(z)$, which are based on the discrete splines, then we can explicitly design tight and semitight frames, where the waveforms are (anti)symmetric and have arbitrary smoothness. The framelets may have any number of vanishing moments. Since there is a relation between the filters and the Butterworth filters, we call the corresponding frames the Butterworth frames. Let us denote $\rho(z) \triangleq z + 2 + z^{-1}$.

Let $F(z) = U_{1,2}^{2m}(z)$. Then,

$$\begin{aligned} G^0(z) = \widetilde{G}^0(z) &= \frac{1 + z^{-1} U_{1,2}^{2m}(z^2)}{\sqrt{2}} = \frac{\sqrt{2}\rho^r(z)}{\rho^r(z) + \rho^r(-z)}, \\ G^2(z) = \widetilde{G}^2(z) &= \frac{1 - z^{-1} U_{1,2}^{2m}(z^2)}{\sqrt{2}} = \frac{\sqrt{2}\rho^r(-z)}{\rho^r(z) + \rho^r(-z)}. \end{aligned} \tag{1.87}$$

We get a tight frame when we factorize $W(z)$ to be

$$W(z) = 1 - \left| U_{1,2}^{2m}(z) \right|^2 = w(z) w\left(\frac{1}{z}\right). \tag{1.88}$$

From (1.84), we have

$$\begin{aligned} W(z^2) = 2G^0(z)G^0(-z) &= \frac{4(-1)^m z^{-2m} (1 - z^2)^{2m}}{\left(\rho^m(z) + \rho^m(-z)\right)^2} = w(z^2) w(z^{-2}), \\ w(z^2) &\triangleq \frac{2(1 - z^2)^m}{\rho^m(z) + \rho^m(-z)}. \end{aligned} \tag{1.89}$$

If $m = 2n$, then we can define $w(z^2)$ differently:

$$w(z^2) \triangleq \frac{2(z - z^{-1})^{2n}}{\rho^{2n}(z) + \rho^{2n}(-z)}. \tag{1.90}$$

Hence, the three filters $G^0(z)$, defined in (1.87), $G^2(z) = H(-z)$, and $G^1(z) \triangleq z^{-1} w(z^2)/\sqrt{2}$, where $w(z^2)$ is defined in (1.89), generate a tight frame in the signal space. The scaling function $\varphi(t)$ and the framelet $\psi^2(t)$ are symmetric, whereas the framelet $\psi^1(t)$ is symmetric when m is even and antisymmetric when m is odd. The framelet $\psi^2(t)$ has $2m$ vanishing moments and the framelet $\psi^1(t)$ has m

vanishing moments. The frequency response of the filter $G^0(z)$ is maximally flat. The frequency response of the filter $G^2(z)$ is a mirrored version of $G^0(z)$. The frequency response of the filter $G^1(z)$ is symmetric about $\omega = \pi/2$ and it vanishes at the points $\omega = 0 (z = 1)$ and $\omega = \pi (z = -1)$.

We have more freedom in the design of the filters $\widetilde{G}^1(z)$ and $G^1(z)$ if we drop the requirement $w(z) = \widetilde{w}(z)$ in the factorization of $W(z)$. Doing so, we arrive at the semitight case. For example, a symmetric factorization of $W(z)$ is possible for either of even and odd values of m:

$$w(z^2) \triangleq \frac{2\left(2 - z^{-2} - z^2\right)^p}{\left(\rho^m(z) + \rho^m(-z)\right)^s}, \quad \widetilde{w}(z^2) \triangleq \frac{\sqrt{2}\left(2 - z^{-2} - z^2\right)^{m-p}}{\left(\rho^m(z) + \rho^m(-z)\right)^{2-s}}, \quad s \in \mathbb{Z}. \tag{1.91}$$

We can get an antisymmetric factorization by choosing an odd p:

$$w(z^2) \triangleq -\frac{2\left(-z^2\right)^{-m}\left(1 - z^2\right)^p}{\left(\rho^m(z) + \rho^m(-z)\right)^s}, \quad \widetilde{w}(z^2) \triangleq \frac{2\left(-z^2\right)^{p-2m}\left(1 - z^2\right)^{2m-p}}{\left(\rho^m(z) + \rho^m(-z)\right)^{2-s}}, \quad s \in \mathbb{Z}. \tag{1.92}$$

With this factorization, we can change the number of vanishing moments in the framelets $\psi^1(t)$ and $\widetilde{\psi}^1(t)$. One option is that one of the filters $G^1(z) = z^{-1}w(z^2)$ or $\widetilde{G}^1(z) = z^{-1}\widetilde{w}(z^2)$ has a finite impulse response. This is achieved if $s \leq 0$ or $s \geq 2$.

1.6.3.2. Frames based on continuous splines

When we use as the prediction filters $F(z)$ the filters $V^p_{1,2}(z)$, which are based on the continuous splines, then the design of tight frames with (anti)symmetric filters $G^1(z)$ is possible only for the cases $p = 2, 3$ (linear and quadratic splines). For the higher orders, the semitight construction is recommended in order to retain symmetry.

We provide examples of filter banks that generate tight and semitight frames.

Example 1.15

Linear spline, $p = 2$:

$$G^0(z) = \frac{z^{-1} + 2 + z}{2\sqrt{2}}, \qquad G^2(z) = \frac{-z^{-1} + 2 - z}{2\sqrt{2}}, \qquad G^1(z) = \frac{\left(z^{-1} - z\right)}{2}. \tag{1.93}$$

The filters are FIR, and therefore, the scaling function $\varphi(t)$ and the framelets $\psi^1(t)$ and $\psi^2(t)$ are compactly supported. The framelet $\psi^2(t)$ has two vanishing moments. The framelet $\psi^1(t)$ is antisymmetric and has one vanishing moment. The scaling function $\varphi(t)$ is the fundamental linear spline.

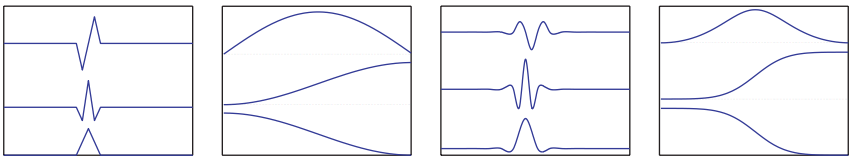

FIGURE 1.13. Filters and framelets for tight frames resulting from the linear spline (two leftmost columns) and continuous quadratic spline (two rightmost columns).

Quadratic continuous spline, $p = 3$ (cubic discrete spline, $m = 2$):

$$G^0(z) = \frac{(z+2+z^{-1})^2}{\sqrt{2}(z^{-2}+6+z^2)}, \qquad G^1(z) = \frac{(z-2+z^{-1})^2}{\sqrt{2}(z^{-2}+6+z^2)}, \tag{1.94}$$
$$G^2(z) = \frac{2z^{-1}(z-z^{-1})^2}{z^{-2}+6+z^2}.$$

The framelet $\psi^2(t)$ has four vanishing moments. The framelet $\psi^1(t)$ is symmetric and has two vanishing moments. All waveforms belong to C^2.

We display in Figure 1.13 filters and framelets for tight frames resulting from linear spline and the continuous quadratic spline. The four rows on the bottom depict the scaling functions $\varphi(t)$ and the frequency response of the lowpass filters $G^0(z)$, the central four rows display the highpass filters $G^2(z)$ and the framelets $\psi^2(t)$, and the upper four rows depict the bandpass filters $G^1(z)$ and the corresponding framelets $\psi^1(t)$.

Discrete spline of sixth order, $m = 3$:

$$G^0(z) = \frac{(z^{-1}+2+z)^3}{\sqrt{2}(6z^2+20+6z^{-2})}, \qquad G^2(z) = G^0(-z), \qquad G^1(z) = \frac{2z^{-1}(1-z^2)^3}{6z^2+20+6z^{-2}}. \tag{1.95}$$

The framelet $\psi^2(t)$ has six vanishing moments. The framelet $\psi^1(t)$ is antisymmetric and has three vanishing moments. All waveforms belong to C^3.

Discrete spline of eighth order, $m = 4$:

$$G^0(z)\frac{(z^{-1}+2+z)^4}{\sqrt{2}(z^{-4}+28z^{-2}+70+28z^2+z^4)}, \qquad G^2(z) = G^0(-z), \tag{1.96}$$
$$G^1(z) = \frac{2z^{-1}(z-z^{-1})^4}{z^{-4}+28z^{-2}+70+28z^2+z^4}.$$

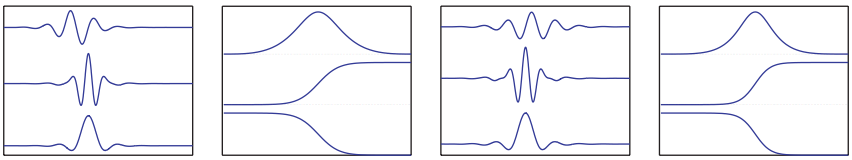

FIGURE 1.14. Filters and framelets for tight frames resulting from the discrete spline of sixth order (two leftmost columns) and the discrete spline of eighth order (two rightmost columns).

The framelet $\psi^2(t)$ has eight vanishing moments. The framelet $\psi^1(t)$ is symmetric and has four vanishing moments. All waveforms belong to C^3.

We display in Figure 1.14 filters and framelets for tight frames resulting from discrete splines of sixth and eighth orders. The figure is organized similarly to Figure 1.13.

Continuous cubic spline, $p = 4$:

$$G^0(z) = \frac{(z^{-1} + 2 + z)^2 (z + 4 + z^{-1})}{8\sqrt{2}(z^{-2} + 4 + z^2)}, \qquad G^2(z) = G^0(-z). \tag{1.97}$$

To obtain the filter $G^0(z)$, the function

$$W(z^2) = 2G^0(z)G^0(-z) = \frac{(z^{-1} - z)^4 (z^2 - 14 + z^{-2})}{8(z^{-2} + 4 + z^2)^2} \tag{1.98}$$

has to be factorized. The factorization $W(z) = w(z)w(1/z)$, which leads to tight frame, results in the filter

$$G^1(z) = z^{-1} \frac{(z^{-1} - z)^2 (1 - qz^2)}{8q\sqrt{2}(z^{-2} + 4 + z^2)}, \tag{1.99}$$

where $q = 7 - 4\sqrt{3} \approx 0.0718$. The filter is not symmetric about inversion $z \to 1/z$, and consequently, the framelet $\psi^1(t)$ is slightly asymmetric. It has two vanishing moments, whereas the framelet $\psi^2(t)$ has four vanishing moments.

We display in Figure 1.15 filters and framelets for tight frame resulting from the continuous cubic spline. The first from the left frame displays the waveforms, the second frame displays the frequency response of the filter bank, and the last frame provides the closed-up view to framelet $\psi^1(t)$ in order to highlight its asymmetry.

The factorization $W(z) = w(z)\widetilde{w}(1/z)$ with unequal factors $w(z)$ and $\widetilde{w}(z)$ leads to a semitight frame. We present the filters $\widetilde{G}^1(z)$ and $G^1(z)$ that result from

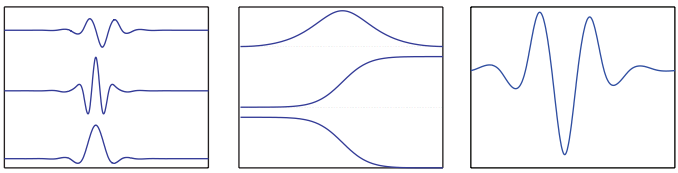

FIGURE 1.15. Filters and framelets for tight frames resulting from the continuous cubic spline (two leftmost columns) and the closed-up view of the framelet $\psi^1(t)$ (rightmost column).

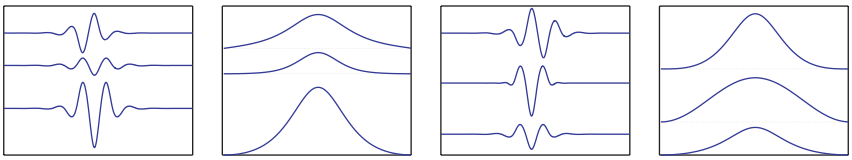

FIGURE 1.16. Filters and framelets for semitight frames resulting from the continuous cubic spline, that correspond to (1.100) (bottom row), (1.101) (central row) and (1.102) (top row).

three different factorization modes:

(1) symmetric factorization with equal number (two) of vanishing moments in the analysis $\widetilde{\psi}^1(t)$ and synthesis $\psi^1(t)$ framelets:

$$\widetilde{G}^1(z) = z^{-1}\frac{(z^{-1}-z)^2}{8\sqrt{2}(z^{-2}+4+z^2)}, \qquad G^1(z) = z^{-1}\frac{(z^{-1}-z)^2(-z^2+14-z^{-2})}{8\sqrt{2}(z^{-2}+4+z^2)}; \tag{1.100}$$

(2) symmetric factorization with equal number (two) of vanishing moments in the analysis $\widetilde{\psi}^1(t)$ and synthesis $\psi^1(t)$ framelets. The analysis filter $\widetilde{G}^1(z)$ is FIR, and consequently, the framelet $\widetilde{\psi}^1(t)$ is compactly supported:

$$\widetilde{G}^1(z) = z^{-1}\frac{(z^{-1}-z)^2}{8\sqrt{2}}, \qquad G^1(z) = z^{-1}\frac{(z^{-1}-z)^2(-z^2+14-z^{-2})}{8\sqrt{2}(z^{-2}+4+z^2)^2}; \tag{1.101}$$

(3) antisymmetric factorization with three vanishing moments in the analysis $\widetilde{\psi}^1(t)$ and one vanishing moment in synthesis $\psi^1(t)$ framelets:

$$\widetilde{G}^1(z) = \frac{(z^{-1}-z)^3}{8\sqrt{2}(z^{-2}+4+z^2)}, \qquad G^1(z) = \frac{(z^{-1}-z)(-z^2+14-z^{-2})}{8\sqrt{2}(z^{-2}+4+z^2)}. \tag{1.102}$$

We recall that the scaling function $\varphi(t)$ is the fundamental cubic spline and all the waveforms in the tight and semitight frames are cubic splines.

We display in Figure 1.16 the filters $\widetilde{G}^1(z)$ and $G^1(z)$ and framelets $\widetilde{\psi}^1(t)$ and $\psi^1(t)$ that result from the above modes of factorization. The four plots on the

bottom depict the analysis framelets $\widetilde{\psi}^1(t)$, the frequency response of the analysis filter $\widetilde{G}^1(z)$, the synthesis framelets $\psi^1(t)$, the frequency response of the synthesis filter $G^1(z)$, respectively, where the filters are given in (1.100). The central four plots do the same for the case (1.101) and the upper four correspond to (1.102).

Remarks 1.16. (1) From the above figures, we see that the designed waveforms are smooth, well localized in time domain, and symmetric. They are as smooth as the synthesis waveforms in the biorthogonal wavelet transforms originating from the same prediction filter and are smoother than the analysis waveforms.

(2) The frequency responses of the filters are maximally flat (has no ripples) in the passband, and roll towards zero in the stopband. As the order of the generating spline is high, the decline is steeper in the stopband.

(3) The frequency responses of the lowpass filter $G^0(z)$ and the highpass filter $G^2(z)$ are monotonous and are the mirrored versions of each other. The bumps, which are present in the filters $\widetilde{H}^0(z)$ and $H^1(z)$ of the wavelet filter bank, are compensated by the bandpass filter $G^1(z)$.

(4) The transfer functions of all designed filters are rational functions. Therefore, the filters (except for the filters derived from the linear spline) have infinite impulse response (IIR). But they can be efficiently implemented via causal-anticausal recursive filtering (see the appendix).

1.7. Erasure recovery properties of the designed wavelet frames

In this section, we outline a scheme that applies the designed wavelet frames to recovery of erasures, which occur when a multimedia signal is transmitted through a lossy channel. This is described in [1].

Conventional methods for protecting data are well developed both in theory and practice. Block and convolutional codes are considered to be very efficient classes as channel codes. They are widely used in wireless and wireline channels such as the Internet. However, these codes, and other conventional methods, do not generally take into account the inner structure of the transmitted (multimedia) signal. Rather, it is assumed that every bit is equally significant, and hence it has to be equally protected. Multimedia information usually undergoes some transform (e.g., DCT, FFT, or wavelet) followed by quantization and lossless compression (entropy coding). The last two operations constitute source coding. The resulting binary sequence (which assumed to be white noise) typically contains bits with unequal significance, which must be protected accordingly. Due to this inhomogeneity, direct application of channel coding methods to audio-visual information is not optimal; it may significantly increase the transmission length if the (equal) error correction code is chosen according to the most vulnerable data. Hence, it is desired to design error correction codes that dynamically allocate more bits to more important information. Such codes are known as unequal error protection (UEP) codes. Due to the growing importance in rich multimedia data transmission, unequal error protection methods have attracted research efforts, see, for example, [30] and the references therein. The designed framelet transform can be

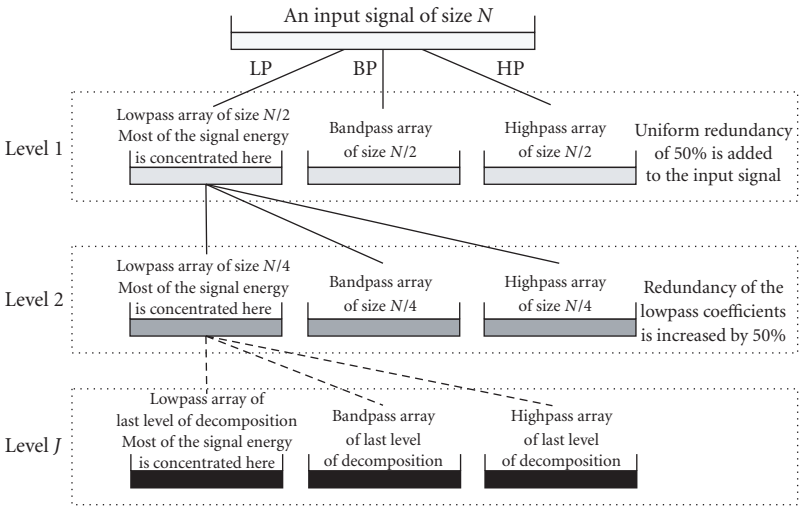

FIGURE 1.17. Diagram of multiscale frame transform with 3-channel filter bank and downsampling factor of 2.

effectively employed as a true combined source-channel coding scheme—there is no separate source coding followed by channel coding. In fact, no explicit channel coding is used. The proposed approach makes use of naturally occurring redundancy within multiscale decomposition of framelet transforms to provide unequal error protection (UEP).

1.7.1. Remarks on unequal error protection

The multiscale frame transform, which is described in Section 1.2.3, is demonstrated schematically in Figure 1.17.

Assume that there are four scales of decomposition. Figure 1.18 displays the spectra of the discrete-time framelets $\psi^{r,1}$ $\psi^{r,2}$, $r = 1, 2, 3, 4$, and φ^4 that originate from the filter bank (1.94). The shifts of these framelets provide a four-scale tight frame expansion of the signal. First scale of decomposition produces three blocks of coefficients: lowpass, bandpass and highpass. As it was explained in Section 1.2.3, these are the coefficients of the orthogonal projections of the signal onto the subspaces spanned by two-sample shifts of the discrete-time framelets $\varphi^1(k)$, $\psi^{1,2}(k)$, and $\psi^{1,1}(k)$, respectively. The spectra of the framelets $\psi^{1,2}(k)$ and $\psi^{1,1}(k)$ are displayed in the top row of Figure 1.18. The second step of the decomposition transforms the lowpass block into three blocks of coefficients, which are the coefficients of the orthogonal projections of the signal onto the subspaces spanned by four-sample shifts of the framelets $\varphi^2(k)$, $\psi^{2,2}(k)$, and $\psi^{2,1}(k)$. The spectra of the framelets $\psi^{2,2}(k)$ and $\psi^{2,1}(k)$ are displayed in the second from the top row of the figure. The last fourth step of the decomposition transforms the lowpass block of the third scale into three blocks of coefficients, which are the coefficients of the orthogonal projections of the signal onto the subspaces spanned

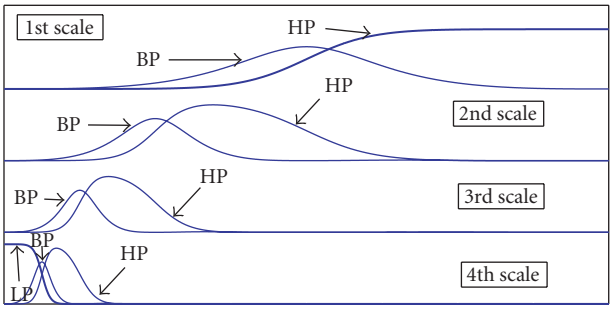

FIGURE 1.18. Spectra of the discrete-time framelets $\psi^{r,1}$, $\psi^{r,2}$, $r = 1, 2, 3, 4$, and φ^4 that originate from the filter bank (1.94). The abbreviation LP means lowpass, it is related to φ^4, HP means highpass, it is related to $\psi^{r,1}$, BP means bandpass, it is related to $\psi^{r,2}$.

by sixteen-sample shifts of the framelets $\varphi^4(k)$, $\psi^{4,2}(k)$, and $\psi^{4,1}(k)$. The spectra of these framelets are displayed in the bottom row of the figure. The reconstruction consists of the synthesis of the original signal from the above set of projections.

We see that the spectra displayed in Figure 1.18 form at least twofold cover of the frequency domain of the signal except for the frequency bands occupied by the spectra of the low-frequency framelet φ^4 and the high-frequency framelet $\psi^{1,1}$. They are highlighted by boldface lines in Figure 1.18. It means that once a projection (except for the projections on φ^4 and $\psi^{1,1}$) is lost, it can be restored from the remaining projections. Also two or more projections, whose spectra do not overlap, can be restored. In other words, erasure of a number of coefficients from a block or even the whole block (except for the blocks related to φ^4 and $\psi^{1,1}$) can be compensated by the coefficients from the remaining blocks.

Two exclusive blocks of coefficients related to φ^4 and $\psi^{1,1}$ must also be protected. The lowpass block is the most significant. Erasure of even one coefficient can essentially distort the signal. But for the four-scale transform, it comprises only $N/16$ coefficients, where N is the length of the signal. If we expand the transform to scale J, then the last lowpass block comprises only $N/2^J$ coefficients. This relatively small number of coefficients can also be protected at a low computational cost.

The highpass block related to $\psi^{1,1}$ is most populated ($N/2$ coefficients). Due to the vanishing moments of the framelets $\psi^{1,1}$, this block contains relatively small number of significant coefficients, which correspond to sharp transients in the signal (edges in the image). Only these significant coefficients deserve an additional protection.

1.7.2. Outline of the recovery algorithm

Assume that the original 2D image is arranged into a 1D array $X \in \mathbb{R}^N$ and the coefficients of its 2D framelet transform are arranged into a 1D array $Y \in \mathbb{H} \subset \mathbb{R}^K$ of length $K > N$. Let $\mathcal{J} \triangleq \{C_k\}_1^{nm}$ be the set of coordinates of this array, and let $E \subset \mathcal{J}$ be the set of coordinates of the erased coefficients. The subspace $\mathbb{H} \subset \mathbb{R}^K$ is called

Initialize $y^{(0)} = \widetilde{Y}$;
for $k = 0$ to $K - 1$
$\hat{x}^{(k)} = Fy^{(k)}$; *fit out-of-interval values into* $[L_0, L_{255}]$;
$\hat{y}^{(k)} = \widetilde{F} * \hat{x}^{(k)}$;
$y^{(k+1)} = \hat{y}^{(k)}$ *on the coordinates of* E;
$y^{(k+1)} = \widetilde{Y}$ *on the coordinates of* $\overline{E}$;
end.

Algorithm 1.1

the space of codewords. Define $\overline{E} \triangleq \mathcal{S} \setminus E$ and $\widetilde{Y}$ is obtained from Y by erasing all coefficients that correspond to E. Let $\widetilde{F}$ be the analysis operator $\widetilde{F} : \mathbb{R}^N \mapsto H \subset \mathbb{R}^K$, $K > N$ associated with the framelet transform: $Y = \widetilde{F}X$. Obviously, $\operatorname{rank}(\widetilde{F}) = N$. Let F be the inverse operator (i.e., the synthesis operator) of $\widetilde{F}$. We denote by $\widetilde{\widetilde{F}}$ the matrix $\widetilde{F}$ with erased rows determined by the coordinates of E. Assume that $\widetilde{Y}$ contains zeros instead of all the erased coefficients in $\widetilde{Y}$. If $\operatorname{rank}(\widetilde{\widetilde{F}}) = N$, then $\widetilde{Y}$ contains sufficient information to recover the original data X.

Each coefficient of the transformed image is presented by few bits. If one or more bits associated with the same coefficient are lost in transit, the whole coefficient may be treated as an erasure, or alternatively, as being in error. It is well known that, in general, recovering from erasures is easier than recovering from errors. Hence the motivation for the algorithm stems. This algorithm is a slightly modified version of the well-known Gerchberg [22] and Papoulis [35] algorithm. The Gerchberg-Papoulis algorithm was applied, in particular, to interpolation of data given on an irregular grid. The application of the mentioned algorithm to erasure recovery was reported in [37].

It utilizes the redundancy inherent in frame transforms to recover from erasures of whole coefficients that occur during transmission. As before, $\widetilde{Y}$ denotes the received set of coefficients with the convention that erased coefficients are substituted by zeros. Let y^k denote the set of (received+recovered) framelet coefficients at iteration k of the recovery algorithm. Assume the image intensities belong to the interval $[L_0, L_{255}]$, where $L_0 < L_{255}$.

This framelet-based algorithm Algorithm 1.1 iteratively recovers an image from its transformed version $\widetilde{Y}$ that contains erasures. The recovered image at each iteration is given by $\hat{x}^{(k)}$.

1.7.3. Experimental results

We conducted a series of experiments on image recovery from erasures of the transform coefficients. This can be regarded as a simulation of channels with erasures. To be specific, we applied the framelet decomposition up to the fourth level. The redundancy factor of this decomposition is 2.66. Then $\alpha \cdot 100\%$ of the transform coefficients, whose locations were randomly chosen, were put to zero. We restored the images using the iterative algorithm described in Section 1.7.2. We

Table 1.5. Averaged PSNR values of the four reconstructed images using symmetric tight frame (1.94), antisymmetric tight frame (1.95), and semitight frame (1.97) and (1.102).

Erasure	10%	20%	30%	40%	50%	60%	70%
PSNR/S-TF	51.8418	50.7470	49.0475	46.3734	40.7849	32.3740	19.2204
PSNR/symm. TF	52.0012	51.3969	50.0345	47.9709	43.6514	32.9655	19.7563
PSNR/antisymm. TF	52.2622	51.3204	50.2554	48.2412	43.1816	32.8288	19.5409

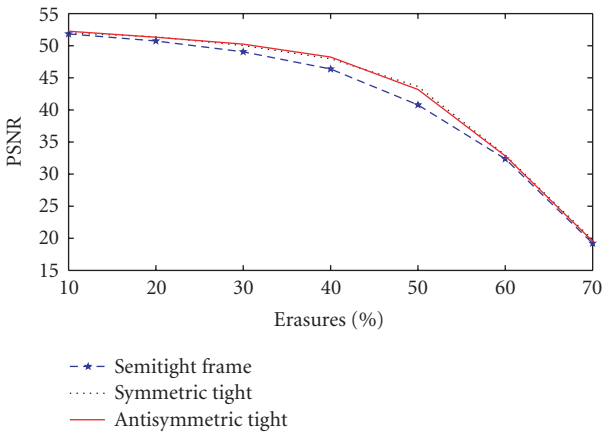

Figure 1.19. Averaged PSNR of the reconstructed images versus coefficient erasure probability.

tested two benchmark images *Barbara* and *boats* and two medical images taken by MRI scanner while using $\alpha = 0.1, 0.2, 0.3, 0.4, 0.5, 0.6, 0.7$. Three different types of framelets were tested: the symmetric tight framelets originating from quadratic spline (1.94), tight frame originating from discrete spline of sixth order, where $\psi^1(t)$ is antisymmetric, (1.95), and the semitight frame originating from cubic spline (1.97) and (1.102), where $\widetilde{\psi}^1(t)$ and $\psi^1(t)$ are antisymmetric. The distance between the original and the restored images was evaluated via PSNR (see (1.77)).

The experimental results are summarized in Table 1.5 and are illustrated by Figure 1.19. The results for all the tested images are similar to each other, therefore, for brevity, we present PSNR values that are averaged over the four images. The results demonstrate a graceful degradation in performance when the erasure probability of the coefficients increases to 0.7. The performance of the symmetric and antisymmetric tight frames is almost identical, while the biframe produces images with a slightly lower PSNR.

In addition, we display the four restored images in Figures 1.20–1.23. All the figures are similarly organized. Each of them comprises three columns. The left column displays the original image, the middle column is the corrupted image, the right column displays the reconstructed image from the corrupted transform coefficients. We observe from the images that the restoration scheme, that is based on the wavelet frames, produces satisfactory output even for 60 percent of randomly

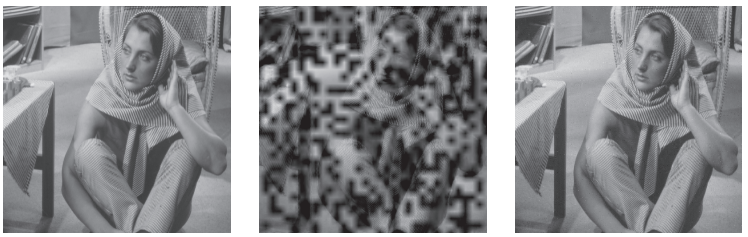

(a) (b) (c)

FIGURE 1.20. Results from the application of the antisymmetric tight framelet transform. (a) Original image, (b) the corrupted image with 60% erased coefficients, (c) the recovered image. PSNR = 32.24.

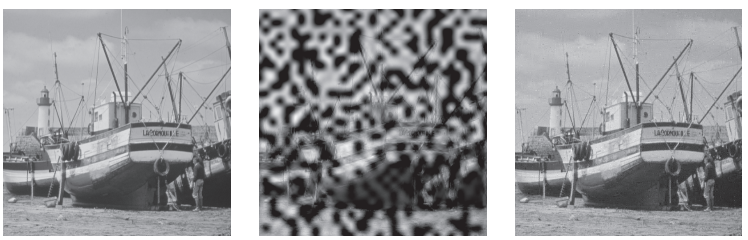

(a) (b) (c)

FIGURE 1.21. Results from the application of the symmetric tight framelet transform. (a) The source image, (b) the corrupted image with 60% erased coefficients, (c) the recovered image. PSNR = 31.98.

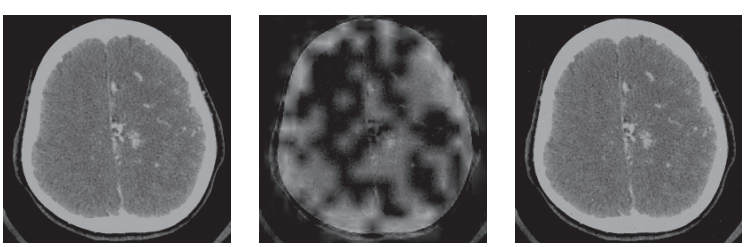

(a) (b) (c)

FIGURE 1.22. Results from the application of symmetric semitight framelet transform. (a) The source image, (b) the corrupted image with 50% erased coefficients, (c) the recovered image. PSNR = 43.354.

erased coefficients. For 50 and, especially, for 40 percents of erased coefficients, the restored images hardly can be distinguished from the original source images.

1.8. Biorthogonal wavelet transforms generated by filter banks with downsampling factor $N = 3$ (triadic transforms)

In this section, we expand the method that constructs biorthogonal wavelet transforms, which was described in Section 1.4, to the case when the downsampling factor of the filter banks is $N = 3$. As in Section 1.4, the construction is carried out via the lifting scheme.

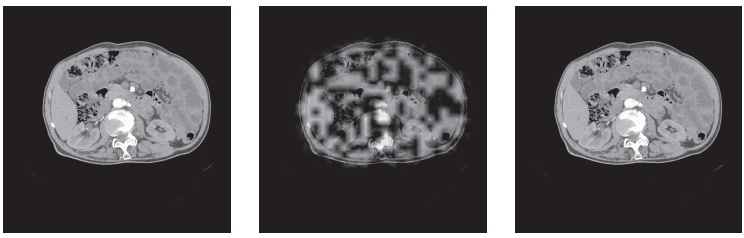

(a) (b) (c)

FIGURE 1.23. Results from the application of the semitight framelet transform. (a) The source image, (b) the corrupted image with 40% erased coefficients, (c) the recovered image. PSNR = 52.461.

1.8.1. Decomposition

1.8.1.1. Lifting steps

Split: we split the signal $\mathbf{x}$ into three subarrays:

$$\mathbf{x}_{-1} \triangleq \{x_{3l-1}\}_{l\in\mathbb{Z}}, \qquad \mathbf{x}_0 \triangleq \{x_{3l}\}_{l\in\mathbb{Z}}, \qquad \mathbf{x}_1 \triangleq \{x_{3l+1}\}_{l\in\mathbb{Z}}. \tag{1.103}$$

Let $X_{-1}(z)$, $X_0(z)$, and $X_1(z)$ denote the z-transforms of these subarrays.

Predict: we predict

$$\check{D}_{-1}(z) = X_{-1}(z) - \widetilde{F}_{-1}(z^{-1})X_0(z), \qquad \check{D}_1(z) = X_1(z) - \widetilde{F}_1(z^{-1})X_0(z). \tag{1.104}$$

Here, $\widetilde{F}_{-1}$ and $\widetilde{F}_1$ are some filters that are applied to the subarray $\mathbf{x}_0$ in order to predict the subarrays $\mathbf{x}_{-1}$ and $\mathbf{x}_1$, respectively. Then, these latter subarrays are replaced by the differences $\check{\mathbf{d}}_{-1}$ and $\check{\mathbf{d}}_1$ between initial and predicted values.

Update: the array $\mathbf{x}_0$ is smoothed using the arrays $\check{\mathbf{d}}_{-1}$ and $\check{\mathbf{d}}_1$, which are processed by the update filters F_{-1} and F_1, respectively,

$$D_0(z) = X_0(z) + \frac{1}{3}F_{-1}(z)\check{D}_{-1}(z) + \frac{1}{3}F_1(z)\check{D}_1(z). \tag{1.105}$$

Symmetrization: the filters $V^p_{\mp 1,3}$ and $U^p_{\mp 1,3}$, derived from the splines in Section 1.3, are used as prediction and update filters. These filters are not symmetric, unlike their sums and differences. Therefore, we apply two additional lifting steps:

$$D_1(z) = \frac{\check{D}_1(z) - \check{D}_{-1}(z)}{2}, \qquad D_{-1}(z) = \check{D}_{-1}(z) + D_1(z) = \frac{\check{D}_1(z) + \check{D}_{-1}(z)}{2}. \tag{1.106}$$

1.8.1.2. Polyphase matrix

The above lifting steps can be represented via the matrix-vector multiplication

$$\begin{pmatrix} D_1(z) \\ D_0(z) \\ D_{-1}(z) \end{pmatrix} = \widetilde{\mathbf{P}}(z^{-1}) \cdot \begin{pmatrix} X_1(z) \\ X_0(z) \\ X_{-1}(z) \end{pmatrix}, \tag{1.107}$$

where

$$\begin{aligned} \widetilde{\mathbf{P}}(z^{-1}) &= \begin{pmatrix} \frac{1}{2} & 0 & \frac{-1}{2} \\ 0 & 1 & 0 \\ \frac{1}{2} & 0 & \frac{1}{2} \end{pmatrix} \cdot \begin{pmatrix} 1 & 0 & 0 \\ \frac{F_1(z)}{3} & 1 & \frac{F_{-1}(z)}{3} \\ 0 & 0 & 1 \end{pmatrix} \cdot \begin{pmatrix} 1 & -\widetilde{F}_1(z^{-1}) & 0 \\ 0 & 1 & 0 \\ 0 & -\widetilde{F}_{-1}(z^{-1}) & 1 \end{pmatrix} \\ &= \begin{pmatrix} \frac{1}{2} & \frac{-\widetilde{F}_1(z^{-1})}{2} + \frac{\widetilde{F}_{-1}(z^{-1})}{2} & \frac{-1}{2} \\ \frac{F_1(z)}{3} & 1 - \frac{F_1(z)\widetilde{F}_1(z^{-1})}{3} - \frac{F_{-1}(z)\widetilde{F}_{-1}(z^{-1})}{3} & \frac{F_{-1}(z)}{3} \\ \frac{1}{2} & \frac{-\widetilde{F}_1(z^{-1})}{2} - \frac{\widetilde{F}_{-1}(z^{-1})}{2} & \frac{1}{2} \end{pmatrix}. \end{aligned} \tag{1.108}$$

1.8.1.3. Analysis filter bank

The above operations are equivalent to the application to the signal $\mathbf{x}$ of the time-reversed filter bank

$$\begin{aligned} \widetilde{H}^1(z) &\triangleq \frac{z^{-1}}{2} + \frac{\widetilde{F}_{-1}(z^3) - \widetilde{F}_1(z^3)}{2} - \frac{z}{2}, \\ \widetilde{H}^0(z) &= \frac{z^{-1}}{3} F_1(z^{-3}) + 1 - \frac{F_1(z^{-3})\widetilde{F}_1(z^3) + F_{-1}(z^{-3})\widetilde{F}_{-1}(z^3)}{3} + \frac{z}{3} F_{-1}(z^{-3}), \\ \widetilde{H}^{-1}(z) &= \frac{z^{-1}}{2} - \frac{\widetilde{F}_{-1}(z^3) + \widetilde{F}_1(z^3)}{2} + \frac{z}{2} \end{aligned} \tag{1.109}$$

followed by downsampling factor 3.

1.8.2. Reconstruction

1.8.2.1. Lifting steps

Undo symmetrization:

$$\begin{aligned} \check{D}_{-1}(z) &= D_{-1}(z) - D_1(z), \\ \check{D}_1(z) &= 2D_1(z) + \check{D}_1(z) = D_{-1}(z) + D_1(z). \end{aligned} \tag{1.110}$$

Undo update:

$$X_0(z) = D_0(z) - \frac{1}{3}F_{-1}(z)\check{D}_{-1}(z) - \frac{1}{3}F_1(z)\check{D}_1(z). \tag{1.111}$$

Undo predict:

$$X_{-1}(z) = \check{D}_{-1}(z) + \widetilde{F}_{-1}(z^{-1})X_0(z), \qquad X_1(z) = \check{D}_1(z) + \widetilde{F}_1(z^{-1})X_0(z). \tag{1.112}$$

Undo split:

$$X(z) = zX_{-1}(z^3) + X_0(z^3) + z^{-1}X_1(z^3). \tag{1.113}$$

1.8.2.2. Polyphase matrix

The above lifting steps can be represented via the matrix-vector multiplication,

$$\begin{pmatrix} X_1(z) \\ X_0(z) \\ X_{-1}(z) \end{pmatrix} = \mathbf{P}(z) \cdot \begin{pmatrix} D_1(z) \\ D_0(z) \\ D_{-1}(z) \end{pmatrix}, \tag{1.114}$$

where

$$\begin{aligned} \mathbf{P}(z) &= \begin{pmatrix} 1 & \widetilde{F}_1(z^{-1}) & 0 \\ 0 & 1 & 0 \\ 0 & \widetilde{F}_{-1}(z^{-1}) & 1 \end{pmatrix} \cdot \begin{pmatrix} 1 & 0 & 0 \\ \dfrac{-F_1(z)}{3} & 1 & \dfrac{-F_{-1}(z)}{3} \\ 0 & 0 & 1 \end{pmatrix} \cdot \begin{pmatrix} 1 & 0 & 1 \\ 0 & 1 & 0 \\ -1 & 0 & 1 \end{pmatrix} \\ &= \begin{pmatrix} 1+\widetilde{F}_1(z^{-1})\dfrac{F_{-1}(z)-F_1(z)}{3} & \widetilde{F}_1(z^{-1}) & 1-\widetilde{F}_1(z^{-1})\dfrac{F_{-1}(z)+F_1(z)}{3} \\ \dfrac{F_{-1}(z)-F_1(z)}{3} & 1 & \dfrac{-(F_{-1}(z)+F_1(z))}{3} \\ -1+\widetilde{F}_{-1}(z^{-1})\dfrac{F_{-1}(z)-F_1(z)}{3} & \widetilde{F}_{-1}(z^{-1}) & 1-\widetilde{F}_{-1}(z^{-1})\dfrac{F_{-1}(z)+F_1(z)}{3} \end{pmatrix}. \end{aligned} \tag{1.115}$$

1.8.2.3. Synthesis filter bank

The above operations are equivalent to the application to the upsampled sets of the transform coefficients $\check{D}_{-1}$, $\check{D}_0$, and $\check{D}_1$ of the filter bank

$$H_1(z) \triangleq z^{-1} - z + \frac{(F_{-1}(z^3) - F_1(z^3))(z^{-1}\widetilde{F}_1(z^{-3}) + 1 + z\widetilde{F}_{-1}(z^{-3}))}{3},$$

$$H_0(z^{-1}) \triangleq z^{-1}\widetilde{F}_1(z^{-3}) + 1 + z\widetilde{F}_{-1}(z^{-3}),$$

$$H_{-1}(z^{-1}) = H_1(z) \triangleq z^{-1} + z - \frac{(F_{-1}(z^3) + F_1(z^3))(z^{-1}\widetilde{F}_1(z^{-3}) + 1 + z\widetilde{F}_{-1}(z^{-3}))}{3}. \tag{1.116}$$

Remark 1.17. All the designed filters are linear phase. The scaling functions $\varphi(t)$ and $\widetilde{\varphi}(t)$ and wavelets $\psi^{-1}(t)$ and $\widetilde{\psi}^{-1}(t)$ are symmetric, whereas the wavelets $\psi^1(t)$ and $\widetilde{\psi}^1(t)$ are antisymmetric.

1.8.3. Filters and wavelets originating from splines

In this section, we exploit the filters $V^p_{\mp 1,3}$ and $U^p_{\mp 1,3}$ derived from the splines in Section 1.3 as the prediction and update filters.

Proposition 1.18. *If the prediction and update filters in the lifting scheme are either derived from a continuous spline of* $F_{\pm 1}(1/z) = V^p_{\pm 1,3}(z) = F_{\pm 1}(z)$ *or from a discrete spline of* $F_{\pm 1}(1/z) = U^p_{\pm 1,3}(z) = F_{\pm 1}(z)$*, then the analysis filters* $\widetilde{H}^1(z)$ *and the synthesis filters* $H^1(z)$ *are bandpass, filters* $\widetilde{H}^1(z)$ *and the synthesis filters* $H^1(z)$ *are bandpass, whereas the filters* $\widetilde{H}^{-1}(z)$ *and* $H^{-1}(z)$ *are highpass and the filters* $\widetilde{H}^0(z)$ *and* $H^0(z)$ *are lowpass.*

1.8.3.1. Continuous splines

Proposition 1.19. *If the prediction and update filters in the lifting scheme* $F_{\pm 1}(1/z) = V^p_{\pm 1,3}(z) = F_{\pm 1}(z)$ *are derived from the continuous spline of order* p*, then*

(1) *the analysis filters* $\widetilde{H}^{\pm 1}(z)$ *and synthesis filters* $H^{\pm 1}(z)$ *have zero of multiplicity not less than* p *at* $z = 1$*;*
(2) *the analysis wavelets* $\widetilde{\psi}^{\pm 1}(t)$ *and synthesis wavelets* $\psi^{\pm 1}(t)$ *have not less than* p *vanishing moments;*
(3) *the filter* $\widetilde{H}^0(z) = 1 + \widetilde{\chi}(z)$ *and the filter* $H^0(z) = 3 + \chi(z)$*, where the functions* $\widetilde{\chi}(z)$ *and* $\chi(z)$ *have zero of multiplicity not less than* p *at* $z = 1$*;*
(4) *if* $p = 2m+1$*, then* $\widetilde{H}^{-1}(z)$, $H^{-1}(z)$, $\widetilde{\chi}(z)$*, and* $\chi(z)$ *have zero of multiplicity* $p + 1$ *at* $z = 1$*;*
(5) *if* $p = 2m + 1$*, then* $\widetilde{\psi}^{-1}(t)$ *and* $\psi^{-1}(t)$ *have* $p + 1$ *vanishing moments;*
(6) *if* $p = 2m$*, then* $\widetilde{H}^1(z)$ *and* $H^1(z)$ *have zero of multiplicity* $p + 1$ *at* $z = 1$*;*
(7) *if* $p = 2m$*, then the wavelets* $\widetilde{\psi}^1(t)$ *and* $\psi^1(t)$ *have* $p + 1$ *vanishing moments;*

(8) *the synthesis scaling function $\varphi(t)$ is the fundamental spline of order p defined in* (1.33). *All the synthesis waveforms are splines of order p.*

Example 1.20

Linear spline: from (1.37), the analysis filter bank is

$$\begin{aligned}
\widetilde{H}^1(z) &= \frac{\left(z^{-1}-z\right)^3}{6},\\
\widetilde{H}^0(z) &= 1-\frac{\left(z-2+z^{-1}\right)\left(4z^2+5z+5z^{-1}+4z^{-2}\right)}{27},\\
\widetilde{H}^{-1}(z) &= -\frac{\left(-z^{-1}+2-z\right)\left(z^2+2z+2z^{-1}+z^{-2}\right)}{6}.
\end{aligned} \tag{1.117}$$

The synthesis filter bank is

$$\begin{aligned}
H^1(z) &= \frac{\left(z-z^{-1}\right)\left(z-2+z^{-1}\right)\left(22+11\left(z+z^{-1}\right)+4\left(z^2+z^{-2}\right)+z^3+z^{-3}\right)}{27},\\
H^0(z) &= \frac{\left(z+1+z^{-1}\right)^2}{3} = 3+\frac{(z+4+1/z)(z-1/z)^2}{3},\\
H^{-1}(z) &= \frac{\left(-z^{-1}+2-z\right)\left(16+22\left(z+z^{-1}\right)+10\left(z^2+z^{-2}\right)+4\left(z^3+z^{-3}\right)+z^4+z^{-4}\right)}{27}.
\end{aligned} \tag{1.118}$$

The transfer functions $\widetilde{H}^1(z)$ and $H^1(z)$ have zero of multiplicity 3 as $z=1$. Consequently, the wavelets $\widetilde{\psi}^1(t)$ and $\psi^1(t)$ have three vanishing moments. The wavelets $\widetilde{\psi}^{-1}(t)$ and $\psi^{-1}(t)$ have two vanishing moments. The synthesis scaling function $\varphi(t)$ is the linear fundamental spline. The analysis waveforms have a fractal shape.

We display in Figure 1.24 the frequency responses of the analysis and synthesis filter banks, which originate from the linear spline and corresponding waveforms. Figures 1.24–1.28 are organized identically. Each figure consists of four columns. The first column from the left displays the analysis scaling function $\widetilde{\varphi}(t)$ and the analysis wavelets $\widetilde{\psi}_1(t)$ (top) and $\widetilde{\psi}_{-1}(t)$ (bottom). The second column from the left displays the frequency responses of the analysis lowpass filter $\widetilde{H}^0(z)$ (center) and of the analysis highpass filters $\widetilde{H}^1(z)$ (top) and $\widetilde{H}^{-1}(z)$ (bottom). Next column displays the synthesis scaling function $\varphi(t)$ (center) and the synthesis wavelets $\psi_1(t)$ (top) and $\psi_{-1}(t)$ (bottom). Last column (rightmost) displays the frequency responses of the synthesis lowpass filter $H^0(z)$ (bottom) and the synthesis highpass filters $H^1(z)$ (top) and $H^{-1}(z)$ (center).

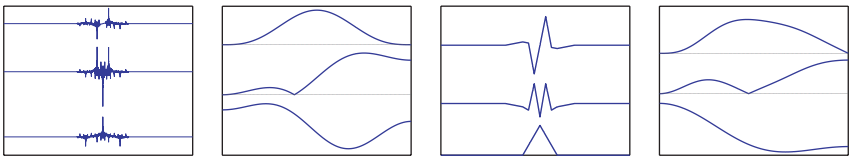

FIGURE 1.24. Filters and wavelets derived from the linear continuous spline.

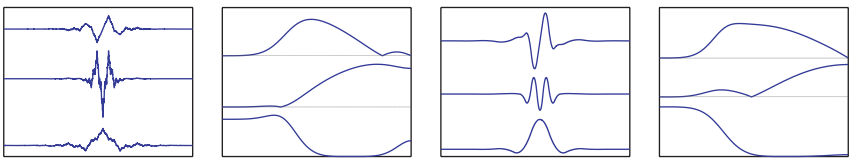

FIGURE 1.25. Filters and wavelets derived from the quadratic continuous spline.

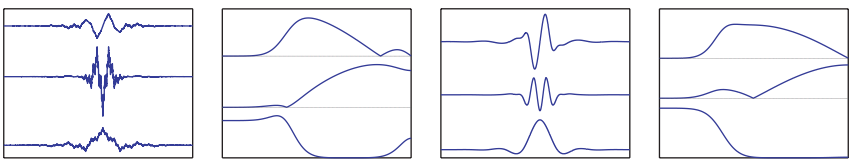

FIGURE 1.26. Filters and wavelets derived from the cubic continuous spline.

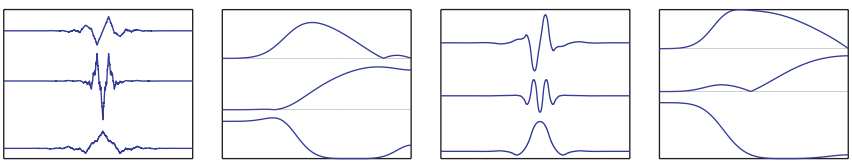

FIGURE 1.27. Filters and wavelets derived from the quadratic discrete spline.

Quadratic spline: from (1.38), we derive the analysis filter bank

$$\widetilde{H}^1(z) = -\frac{(z^{-1}-2+z)(z-z^{-1})(3z^2-2z-7-2z^{-1}+3z^{-2})}{6(z^3+7+z^{-3})},$$

$$\widetilde{H}^0(z) = 1+\frac{(z^{-1}-2+z)^2}{(z^3+7+z^{-3})^2}\sum_{l=0}^{5}\widetilde{c}_l^{\,0}(z^l+z^{-l}), \tag{1.119}$$

$$\widetilde{H}^{-1}(z) = \frac{(z^{-1}-2+z)^2(9z^2+10z-5+10z^{-1}+9z^{-2})}{18(z^3+7+z^{-3})}.$$

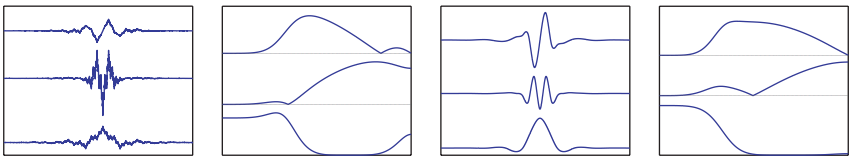

FIGURE 1.28. Filters and wavelets derived from the cubic discrete spline.

The synthesis filter bank is

$$H^1(z) = -\frac{(z^{-1}-2+z)(z-z^{-1})}{(z^3+6+z^{-3})^2}\sum_{l=0}^{5} c_l^1 (z^l + z^{-l}),$$

$$H^0(z) = \frac{(z+6+z^{-1})(z+1+z^{-1})^3}{9(z^3+6+z^{-3})} = 3+\frac{(z-z^{-1})^4(z^2-14z-37-14z^{-1}+z^{-2})}{9(z^3+6+z^{-3})},$$

$$H^{-1}(z) = \frac{2(z^{-1}-2+z)^2}{(z^3+6+z^{-3})^2}\sum_{l=0}^{5} c_l^{-1}(z^l + z^{-l}). \tag{1.120}$$

The transfer functions $\widetilde{H}^1(z)$ and $H^1(z)$ have zero of multiplicity 3 as $z = 1$. Consequently, the wavelets $\widetilde{\psi}^1(t)$ and $\psi^1(t)$ have three vanishing moments. The transfer functions $\widetilde{H}^1(z)$ and $H^1(z)$ have zero of multiplicity 4 at $z = 1$. The wavelets $\widetilde{\psi}^{-1}(t)$ and $\psi^{-1}(t)$ have four vanishing moments. The synthesis scaling function $\varphi(t)$ is the quadratic fundamental spline and the synthesis wavelets are quadratic splines. The analysis waveforms are continuous (C^0) but do not have continuous derivative.

We display in Figure 1.25 the frequency responses of the analysis and synthesis filter banks, which originate from the quadratic continuous spline and corresponding waveforms. This figure is organized similarly to Figure 1.24.

Cubic spline: from (1.39), we derive the analysis filter bank

$$\widetilde{H}^1(z) = \frac{(z^{-1}-2+z)^2(z-z^{-1})(z^3+4z^2-16z-32-16z^{-1}+4z^{-2}+z^{-3})}{54(z^3+4+z^{-3})},$$

$$\widetilde{H}^0(z) = 1-\frac{(z^{-1}-2+z)^2}{2187(z^3+4+z^{-3})^2}\sum_{l=0}^{7}\widetilde{c}_l^0(z^l+z^{-l}),$$

$$\widetilde{H}^{-1}(z) = -\frac{(z^{-1}-2+z)^2(z^4+4z^3-17z^2-20z+10-20z^{-1}-17z^{-2}+4z^{-3}+z^{-4})}{54(z^3+4+z^{-3})}. \tag{1.121}$$

The synthesis filter bank is

$$
\begin{aligned}
H^1(z) &= \frac{\left(z^{-1}-2+z\right)^2\left(z-z^{-1}\right)}{2187\left(z^3+4+z^{-3}\right)^2}\sum_{l=0}^{8} c_l^1\left(z^l+z^{-l}\right),\\
H^0(z) &= \frac{\left(z+4+z^{-1}\right)\left(z+1+z^{-1}\right)^4}{27\left(z^3+4+z^{-3}\right)}\\
&= 3+\frac{\left(z-z^{-1}\right)^4\left(z^3+12z^2-12z-56-12z^{-1}+12z^{-2}+z^{-3}\right)}{27\left(z^3+4+z^{-3}\right)},\\
H^{-1}(z) &= -\frac{\left(z^{-1}-2+z\right)^2}{2187\left(z^3+4+z^{-3}\right)^2}\sum_{l=0}^{9} c_l^{-1}\left(z^l+z^{-l}\right).
\end{aligned}
\tag{1.122}
$$

The transfer functions $\widetilde{H}^1(z)$ and $H^1(z)$ have zero of multiplicity 5 at $z=1$. Consequently, the wavelets $\widetilde{\psi}^1(t)$ and $\psi^1(t)$ have five vanishing moments. The transfer functions $\widetilde{H}^1(z)$ and $H^1(z)$ have zero of multiplicity 4 at $z=1$. The wavelets $\widetilde{\psi}^{-1}(t)$ and $\psi^{-1}(t)$ have four vanishing moments. The synthesis scaling function $\varphi(t)$ is the cubic fundamental spline and the synthesis wavelets are cubic splines. The analysis waveforms are continuous (C^0) but do not have continuous derivative.

We display in Figure 1.26 frequency responses of the analysis and synthesis filter banks, which originate from the cubic continuous spline and the corresponding waveforms. This figure is organized similarly to Figure 1.24.

1.8.3.2. Discrete splines

Proposition 1.21. *If the prediction and update filters in the lifting scheme* $F_{\pm1}(1/z)=U^p_{\pm1,3}(z)=F_{\pm1}(z)$ *are derived from the continuous spline of order* p*, then*

(1) *the analysis filters* $\widetilde{H}^{\pm1}(z)$ *and synthesis filters* $H^{\pm1}(z)$ *have zero of multiplicity not less than* p *at* $z=1$*;*
(2) *the analysis wavelets* $\widetilde{\psi}^{\pm1}(t)$ *and synthesis wavelets* $\psi^{\pm1}(t)$ *have not less than* p *vanishing moments;*
(3) *the filter* $\widetilde{H}^0(z)=1+\widetilde{\chi}(z)$ *and the filter* $H^0(z)=3+\chi(z)$*, where the functions* $\widetilde{\chi}(z)$ *and* $\chi(z)$ *have zero of multiplicity not less than* p *at* $z=1$*;*
(4) *if* $p=2m+1$*, then* $\widetilde{H}^{-1}(z)$, $H^{-1}(z)$, $\widetilde{\chi}(z)$, *and* $\chi(z)$ *have zero of multiplicity* $p+1$ *at* $z=1$*;*
(5) *if* $p=2m+1$*, then* $\widetilde{\psi}^{-1}(t)$ *and* $\psi^{-1}(t)$ *have* $p+1$ *vanishing moments;*
(6) *if* $p=2m$*, then* $\widetilde{H}^1(z)$ *and* $H^1(z)$ *have zero of multiplicity* $p+1$ *at* $z=1$*;*
(7) *if* $p=2m$*, then the wavelets* $\widetilde{\psi}^1(t)$ *and* $\psi^1(t)$ *have* $p+1$ *vanishing moments.*

Quadratic discrete spline: from (1.56), we derive the analysis filter bank

$$\widetilde{H}^1(z) = \frac{(z^{-1}-2+z)(z-z^{-1})(z^2-z-3-z^{-1}+z^{-2})}{6(z^3+7+z^{-3})},$$

$$\widetilde{H}^0(z) = 1+\frac{3(z^{-1}-2+z)^2(z^3+6z^2+6z+1+6z^{-2}+6z^{-2}+z^{-3})}{(z^3+7+z^{-3})^2}\sum_{l=0}^{5}\widetilde{c}_l^0(z^l+z^{-l}),$$

$$\widetilde{H}^{-1}(z) = \frac{(z^{-1}-2+z)^2(z^2+z-1+z^{-1}+z^{-2})}{(z^3+7+z^{-3})}. \tag{1.123}$$

The synthesis filter bank is

$$H^1(z) = -\frac{(z^{-1}-2+z)(z-z^{-1})}{(z^3+7+z^{-3})^2}\sum_{l=0}^{5}c_l^1(z^l+z^{-l}),$$

$$H^0(z) = \frac{(z+1+z^{-1})^3}{z^3+7+z^{-3}} = 3+\frac{(z^{-1}-2+z)^2(2z+5z+z^{-1}+z^{-2})}{(z^3+7+z^{-3})}, \tag{1.124}$$

$$H^{-1}(z) = \frac{(z^{-1}-2+z)^2}{(z^3+7+z^{-3})^2}\sum_{l=0}^{5}c_l^{-1}(z^l+z^{-l}).$$

The transfer functions $\widetilde{H}^1(z)$ and $H^1(z)$ have zero of multiplicity 3 at $z=1$. Consequently, the wavelets $\widetilde{\psi}^1(t)$ and $\psi^1(t)$ have three vanishing moments. The transfer functions $\widetilde{H}^1(z)$ and $H^1(z)$ have zero of multiplicity 4 at $z=1$. The wavelets $\widetilde{\psi}^{-1}(t)$ and $\psi^{-1}(t)$ have four vanishing moments. The synthesis waveforms are continuous and have continuous derivative (C^1). The analysis waveforms are continuous (C^0) but do not have continuous derivative.

We display in Figure 1.27 frequency responses of the analysis and synthesis filter banks, which originate from the quadratic discrete spline and the corresponding waveforms. This figure is organized similarly to Figure 1.24.

Cubic discrete spline: from (1.57), we derive the analysis filter bank

$$\widetilde{H}^1(z) = \frac{(z^{-1}-2+z)^2(z-z^{-1})(4z^3+7+4z^{-3})}{4z^3+19+4z^{-3}},$$

$$\widetilde{H}^0(z) = 1-\frac{(z^{-1}-2+z)^2(4(z^5+z^{-5})-4(z^4+z^{-4})+123(z^3+z^{-3})+120(z+z^{-1}))}{3(4z^3+19+4z^{-3})^2},$$

$$\widetilde{H}^{-1}(z) = \frac{(z^{-1}-2+z)^2(4z^2+5z+5z^{-1}+4z^{-2})}{4z^3+19+4z^{-3}}. \tag{1.125}$$

The synthesis filter bank is

$$H^1(z) = -3\frac{\left(z^{-1}-2+z\right)^2\left(z-z^{-1}\right)}{\left(4z^3+19+4z^{-3}\right)^2}\sum_{l=0}^{4} c_l^1\left(z^l+z^{-l}\right),$$

$$H^0(z) = \frac{\left(z+1+z^{-1}\right)^4}{4z^3+19+4z^{-3}} = 3+\frac{\left(z-z^{-1}\right)^4\left(z^2-4z-12-4z^{-1}+z^{-2}\right)}{4z^3+19+4z^{-3}},$$

$$H^{-1}(z) = \frac{\left(z^{-1}-2+z\right)^2}{\left(4z^3+19+4z^{-3}\right)^2}\sum_{l=0}^{5} c_l^{-1}\left(z^l+z^{-l}\right). \tag{1.126}$$

The transfer functions $\widetilde{H}^1(z)$ and $H^1(z)$ have zero of multiplicity 5 at $z = 1$. Consequently, the wavelets $\widetilde{\psi}^1(t)$ and $\psi^1(t)$ have five vanishing moments. The transfer functions $\widetilde{H}^1(z)$ and $H^1(z)$ have zero of multiplicity 4 at $z = 1$.The wavelets $\widetilde{\psi}^{-1}(t)$ and $\psi^{-1}(t)$ have four vanishing moments. The synthesis waveforms are continuous and have two continuous derivatives (C^2). The analysis waveforms are continuous (C^0) but do not have continuous derivative.

We display in Figure 1.28 frequency responses of the analysis and synthesis filter banks, which originate from the cubic discrete spline and the corresponding waveforms. This figure is organized similarly to Figure 1.24.

Remarks 1.22. (1) The waveforms and the shape of the frequency responses of filters resulting from the discrete splines are very similar to their counterparts that stem from the continuous splines, although the structure of the filters resulting from the discrete splines is simpler.

(2) Unlike dyadic wavelet transforms, one step of the presented transform splits the frequency domain into three subbands. Three waveforms participate in the expansion of a signal. This promises better adaptivity of the expansion to the properties of the signal.

(3) A useful property of the transforms derived from the continuous splines is that the signal waveforms are splines.

(4) Currently, we investigate possible application of the presented transforms to compression and denoising.

Appendix

Implementation of recursive filters

Let $\mathbf{x} = \{x(k)\}$, $k = 1,\ldots,N$. To implement correctly recursive filtering of this finite-length signal, we have to extend $\mathbf{x}$ beyond the given interval. Since our filter banks are symmetric, we use the **HH** extension as in the terminology of [11]. It means that the signal is extended symmetrically with repetition of boundary

samples through both ends of the interval. Namely, $x(0) \triangleq x(1), x(-1) \triangleq x(2), \ldots,$ $x(-k) \triangleq x(k+1)$ and $x(N+1) \triangleq x(N), x(N+2) \triangleq x(N-1), \ldots, x(N+k) \triangleq$ $x(N-k+1)$. This results in periodization of the signal with period $2N$. This extended signal is denoted by $\tilde{\mathbf{x}}$.

Many recursive filters presented in the paper comprise a block of type

$$F(z) = \frac{1+z}{(1+\alpha z)(1+\alpha z^{-1})}. \tag{A.1}$$

We describe the application of the filter F, whose transfer function is given by $F(z)$, to a finite-length signal $\mathbf{x}$:

$$y(z) = F(z)x(z). \tag{A.2}$$

Equation (A.1) is equivalent to

$$F(z) = \frac{1}{1+\alpha}\left(\frac{1}{1+\alpha z^{-1}} + \frac{z}{1+\alpha z}\right). \tag{A.3}$$

Denote

$$\begin{aligned} y_1(z) &= \frac{1}{1+\alpha z^{-1}}x(z) = \sum_{n=0}^{\infty}(-\alpha)^n z^{-n}\tilde{x}(z), \\ y_2(z) &= \frac{z}{1+\alpha z}x(z) = \sum_{n=0}^{\infty}(-\alpha)^n z^{n+1}\tilde{x}(z). \end{aligned} \tag{A.4}$$

Then

$$y_1(k) = x(k) - \alpha y_1(k-1), \qquad y_2(k) = x(k+1) - \alpha y_2(k+1), \tag{A.5}$$

$$\Longleftrightarrow y_1(k) = \tilde{x}(k) + \sum_{n=1}^{\infty}(-\alpha)^n \tilde{x}(k-n), \qquad y_2(k) = \tilde{x}(k+1) + \sum_{n=1}^{\infty}(-\alpha)^n \tilde{x}(k+n+1). \tag{A.6}$$

We can use (A.5) for the computation of $y_1(k)$ and $y_2(k)$ provided that we know $y_1(1)$ and $y_2(N)$, respectively. To evaluate these samples, we employed (A.6) keeping in mind the extension of the input signal $\mathbf{x}$. We have

$$y_1(1) = x(1) + \sum_{n=1}^{\infty}(-\alpha)^n \tilde{x}(-n+1) \approx x(1) + \sum_{n=1}^{d}(-\alpha)^n x(n), \tag{A.7}$$

$$y_2(N) = \tilde{x}(N+1) + \sum_{n=1}^{\infty}(-\alpha)^n \tilde{x}(N+n+1) \approx x(N) + \sum_{n=1}^{d}(-\alpha)^n x(N-n), \tag{A.8}$$

where d is the prescribed initialization depth.

Filtering (A.2) can be implemented by the following parallel algorithm:

(1) evaluate $y_1(1)$ from (A.7) and $y_2(N)$ from (A.8);
(2) calculate $y_1(k) = x(k) - \alpha y_1(k-1)$, $k = 2, \ldots, N$, and $y_2(k) = x(k+1) - \alpha y_2(k+1)$, $k = N-1, \ldots, 1$;
(3) $y(k) = (y_1(k) + y_2(k))/(1+\alpha)$, $k = 1, \ldots, N$.

Equations (A.6) and (A.8) imply that $y_2(N) = y_1(N)$. Hence, it follows that

$$y(N) = \frac{y_1(N) + y_2(N)}{1+\alpha} = \frac{2y_1(N)}{1+\alpha}. \tag{A.9}$$

The cascade algorithm has the following form:

(1) evaluate $y_1(1)$ from (A.7);
(2) calculate $y_1(k) = x(k) - \alpha y_1(k-1)$, $k = 2, \ldots, N$;
(3) evaluate $y(N)$ from (A.9);
(4) calculate $y(k) = y_1(k) + y_1(k+1) - \alpha y(k+1)$, $k = N-1, \ldots, 1$.

Bibliography

[1] O. Amrani, A. Z. Averbuch, T. Cohen, and V. A. Zheludev, "Symmetric interpolatory framelets and their error correction properties," to appear in *International Journal of Wavelets, Multiresolution and Information Processing*.

[2] A. Z. Averbuch and V. A. Zheludev, "Construction of biorthogonal discrete wavelet transforms using interpolatory splines," *Applied and Computational Harmonic Analysis*, vol. 12, no. 1, pp. 25–56, 2002.

[3] A. Z. Averbuch, A. B. Pevnyi, and V. A. Zheludev, "Biorthogonal butterworth wavelets derived from discrete interpolatory splines," *IEEE Transactions on Signal Processing*, vol. 49, no. 11, pp. 2682–2692, 2001.

[4] A. Z. Averbuch, A. B. Pevnyi, and V. A. Zheludev, "Butterworth wavelet transforms derived from discrete interpolatory splines: recursive implementation," *Signal Processing*, vol. 81, no. 11, pp. 2363–2382, 2001.

[5] A. Z. Averbuch and V. A. Zheludev, "Wavelets transforms generated by splines," to appear in *International Journal of Wavelets, Multiresolution, and Information Processing*.

[6] A. Z. Averbuch and V. A. Zheludev, "Lifting scheme for biorthogonal multiwavelets originated from hermite splines," *IEEE Transactions on Signal Processing*, vol. 50, no. 3, pp. 487–500, 2002.

[7] A. Z. Averbuch and V. A. Zheludev, "A new family of spline-based biorthogonal wavelet transforms and their application to image compression," *IEEE Transactions on Image Processing*, vol. 13, no. 7, pp. 993–1007, 2004.

[8] A. Z. Averbuch, V. A. Zheludev, and T. Cohen, "Multiwavelet frames in signal space originated from hermite splines," to appear in *IEEE Transactions on Signal Processing*.

[9] A. Z. Averbuch, V. A. Zheludev, and T. Cohen, "Interpolatory frames in signal space," *IEEE Transactions on Signal Processing*, vol. 54, no. 6, part 1, pp. 2126–2139, 2006.

[10] A. Z. Averbuch, V. A. Zheludev, and T. Cohen, "Tight and sibling frames originated from discrete splines," *Signal Processing*, vol. 86, no. 7, pp. 1632–1647, 2006.

[11] C. M. Brislawn, "Classification of nonexpansive symmetric extension transforms for multirate filter banks," *Applied and Computational Harmonic Analysis*, vol. 3, no. 4, pp. 337–357, 1996.

[12] R. H. Chan, S. D. Riemenschneider, L. Shen, and Z. Shen, "High-resolution image reconstruction with displacement errors: a framelet approach," *International Journal of Imaging Systems and Technology*, vol. 14, no. 3, pp. 91–104, 2004.

[13] R. H. Chan, S. D. Riemenschneider, L. Shen, and Z. Shen, "Tight frame: an efficient way for high-resolution image reconstruction," *Applied and Computational Harmonic Analysis*, vol. 17, no. 1, pp. 91–115, 2004.

[14] C. K. Chui and W. He, "Compactly supported tight frames associated with refinable functions," *Applied and Computational Harmonic Analysis*, vol. 8, no. 3, pp. 293–319, 2000.

[15] A. Cohen, I. Daubechies, and J. C. Feauveau, "Biorthogonal bases of compactly supported wavelets," *Communications on Pure and Applied Mathematics*, vol. 45, no. 5, pp. 485–560, 1992.

[16] Z. Cvetković and M. Vetterli, "Oversampled filter banks," *IEEE Transactions on Signal Processing*, vol. 46, no. 5, pp. 1245–1255, 1998.

[17] D. Marpe, G. Heising, H. L. Cycon, and A. P. Petukhov, "Video coding using a bilinear image warping motion model and wavelet-based residual coding," in *Wavelet Applications in Signal and Image Processing VII*, vol. 3813 of *Proceedings of SPIE*, pp. 401–408, Denver, Colo, USA, 1999.

[18] I. Daubechies, "Orthonormal bases of compactly supported wavelets," *Communications on Pure and Applied Mathematics*, vol. 41, no. 7, pp. 909–996, 1988.

[19] I. Daubechies, *Ten Lectures on Wavelets*, SIAM, Philadelphia, Pa, USA, 1992.

[20] I. Daubechies, B. Han, A. Ron, and Z. Shen, "Framelets: MRA-based constructions of wavelet frames," *Applied and Computational Harmonic Analysis*, vol. 14, no. 1, pp. 1–46, 2003.

[21] F. Labeau, J.-C. Chiang, M. Kieffer, P. Duhamel, L. Vandendorpe, and B. Macq, "Oversampled filter banks as error correcting codes: theory and impulse noise correction," *IEEE Transactions on Signal Processing*, vol. 53, no. 12, pp. 4619–4630, 2005.

[22] R. W. Gerchberg, "Super-resolution through error energy reduction," *Optica Acta*, vol. 21, no. 9, pp. 709–720, 1974.

[23] V. K. Goyal, J. Kovacevic, and J. A. Kelner, "Quantized frame expansions with erasures," *Applied and Computational Harmonic Analysis*, vol. 10, no. 3, pp. 203–233, 2001.

[24] V. K. Goyal, M. Vetterli, and N. T. Thao, "Quantized overcomplete expansions in $\mathbb{R}^n$: analysis, synthesis, and algorithms," *IEEE Transactions on Information Theory*, vol. 44, no. 1, pp. 16–31, 1998.

[25] G. Rath and C. Guillemot, "Characterization of a class of error correcting frames for robust signal transmission over wireless communication channels," *EURASIP Journal on Applied Signal Processing*, vol. 2005, no. 2, pp. 229–241, 2005.

[26] H. Bölcskei, F. Hlawatsch, and H. G. Feichtinger, "Frame-theoretic analysis of oversampled filter banks," *IEEE Transactions on Signal Processing*, vol. 46, no. 12, pp. 3256–3268, 1998.

[27] C. Herley and M. Vetterli, "Wavelets and recursive filter banks," *IEEE Transactions on Signal Processing*, vol. 41, no. 8, pp. 2536–2556, 1993.

[28] Q. Jiang, "Parameterizations of masks for tight affine frames with two symmetric/antisymmetric generators," *Advances in Computational Mathematics*, vol. 18, no. 2–4, pp. 247–268, 2003.

[29] J. Kovavectorcević, P. L. Dragotti, and V. K. Goyal, "Filter bank frame expansions with erasures," *IEEE Transactions on Information Theory*, vol. 48, no. 6, pp. 1439–1450, 2002.

[30] C. Lan, K. R. Narayanan, and Z. Xiong, "Scalable image transmission using rate-compatible irregular repeat accumulate (IRA) codes," in *Proceedings of IEEE International Conference on Image Processing (ICIP '02)*, vol. 3, pp. 717–720, Rochester, NY, USA, June 2002.

[31] M. Antonini, M. Barlaud, P. Mathieu, and I. Daubechies, "Image coding using wavelet transform," *IEEE Transactions of Image Processing*, vol. 1, no. 2, pp. 205–220, 1992.

[32] S. Marinkovic and C. Guillemot, "Joint source-channel coding based on cosine-modulated filter banks for erasure-resilient signal transmission," *EURASIP Journal on Applied Signal Processing*, vol. 2005, no. 4, pp. 510–524, 2005.

[33] R. Motwani and C. Guillemot, "Tree-structured oversampled filterbanks as joint source-channel codes: application to image transmission over erasure channels," *IEEE Transactions on Signal Processing*, vol. 52, no. 9, pp. 2584–2599, 2004.

[34] A. V. Oppenheim and R. W. Schafer, *Discrete-Time Signal Processing*, Prentice-Hall, Englewood Cliffs, NJ, USA, 1989.

[35] A. Papoulis, "A new algorithm in spectral analysis and band-limited extrapolation," *IEEE Transactions on Circuits and Systems*, vol. 22, no. 9, pp. 735–742, 1975.

[36] A. P. Petukhov, "Biorthogonal wavelet bases with rational masks and their applications," *Trudy Sankt-Peterburgskogo Matematicheskogo Obshchestva*, vol. 7, pp. 168–193, 1999.

[37] A. P. Petukhov, "Wavelet frames and their applications to wireless transmission," in *Proceedings of Communication at the 5th AFA Conference on Curves and Surfaces*, Saint Malo, France, June–July 2002.

[38] A. P. Petukhov, "Symmetric framelets," *Constructive Approximation*, vol. 19, no. 1, pp. 309–328, 2003.

[39] A. Ron and Z. Shen, "Affine Systems in $l^2(\mathbb{R}^d)$ ii: dual systems," *Journal of Fourier Analysis and Applications*, vol. 3, no. 5, pp. 617–637, 1997.

[40] A. Ron and Z. Shen, "Compactly supported tight affine spline frames in $l^2(\mathbb{R}^d)$," *Mathematics of Computation*, vol. 67, no. 221, pp. 191–207, 1998.

[41] A. Said and W. A. Pearlman, "A new, fast, and efficient image codec based on set partitioning in hierarchical trees," *IEEE Transactions on Circuits and Systems for Video Technology*, vol. 6, no. 3, pp. 243–250, 1996.

[42] I. W. Selesnick and A. F. Abdelnour, "Symmetric wavelet tight frames with two generators," *Applied and Computational Harmonic Analysis*, vol. 17, no. 2, pp. 211–225, 2004.

[43] G. Strang and T. Nguen, *Wavelets and Filter Banks*, Wellesley-Cambridge Press, Ellesley, Mass, USA, 1996.

[44] W. Sweldens, "The lifting scheme: a custom-design construction of biorthogonal wavelets," *Applied and Computational Harmonic Analysis*, vol. 3, no. 2, pp. 186–200, 1996.

Amir Z. Averbuch: The School of Computer Science, Tel Aviv University, Tel Aviv 69978, Israel
Email: amir1@post.tau.ac.il

Valery A. Zheludev: The School of Computer Science, Tel Aviv University, Tel Aviv 69978, Israel
Email: zhel@post.tau.ac.il